

THESIS FOR THE DEGREE OF LICENTIATE OF ENGINEERING

Properties of oxygen carriers based on natural and waste
materials at high degrees of reduction

VICTOR PURNOMO

Department of Chemistry and Chemical Engineering

CHALMERS UNIVERSITY OF TECHNOLOGY

Gothenburg, Sweden 2022

Properties of oxygen carriers based on natural and waste materials at high degrees of reduction

VICTOR PURNOMO

© VICTOR PURNOMO, 2022.

Licentiatuppsatser vid Institutionen för Kemi och kemiteknik
Chalmers tekniska högskola
Nr 2022:08

Department of Chemistry and Chemical Engineering
Chalmers University of Technology
SE-412 96 Gothenburg
Sweden
Telephone + 46 (0)31-772 1000

Printed by Chalmers Reproservice
Gothenburg, Sweden 2022

Abstract

Oxygen carriers play an important role in multiple energy conversion processes, such as chemical-looping technology and oxygen-carrier-aided combustion. This thesis particularly explores how a high reduction degree of an oxygen carrier can affect its performance. Oxygen carriers do not usually suffer from a high reduction degree in a normal operation of the widely known chemical-looping combustion. Still, high degrees of reduction may appear locally or during unoptimized conditions, as well as when partial oxidation of fuel is required, such as in chemical-looping gasification. This may lead to performance issues such as lowered reactivity, particle breakage, bed agglomeration, or even defluidization. The main experiments in this thesis were performed in a fluidized bed batch reactor, where it is possible to alternate the feeding of oxidizing and reducing gases, thus mimicking the situation of the air and fuel reactors in a real chemical-looping setup. All oxygen carriers studied here were non-synthesized, either from natural ores or industrial by-products, and are thus inexpensive.

The reactivity of the oxygen carriers toward relevant gaseous fuels is an important parameter. It was found that the syngas conversion decreased at higher reduction degrees of oxygen carriers. The by-products, which contain a lower iron content, saw a quicker decrease of syngas conversion compared to that of the ore-based materials. The same trend was seen on the methane conversion. The decrease seen toward different fuels was due to the exhaustion of the available oxygen in the oxygen carrier particles.

The fluidization performance of the bed particles is critical in a fluidized bed setup, a common arrangement for chemical-looping processes. Defluidization was observed on oxygen carriers based on iron ore materials at higher reduction degrees set by syngas, while the iron-based by-products and manganese ores did not defluidize at all. This was caused by the formation of wüstite and/or elemental iron under a highly reducing environment, which later migrated to the particles' surface and triggered bed agglomeration. Manganese ores seem to be less prone to defluidization compared to the iron ores under highly reducing environment.

The conversion of pine forest residue char, a biomass-based fuel, was investigated at high reduction degrees using ilmenite and iron sand. The hydrogen partial pressure in the bed during the char conversion increased as the oxygen carrier reduction degree increased. The increasing hydrogen partial pressure caused a hydrogen inhibition effect, which subsequently slowed down the char conversion rate. The increasing hydrogen partial pressure was possibly caused by the equilibrium shifting in the water-gas shift reaction and/or the decreasing reactivity of the oxygen carriers themselves. The mass conversion degree thereby affected the char conversion indirectly. There was no significant difference between the reactivity of the char with ilmenite and that with iron sand at higher reduction degrees.

Given these findings, high reduction degrees of oxygen carriers during a chemical-looping operation should preferably be avoided to minimize the risk of performance issues. Despite this, the performance of several oxygen carriers would probably not be affected significantly by a highly reducing environment alone.

Keywords: oxygen carrier, high reduction, reactivity, defluidization, chemical-looping gasification

Acknowledgments

I would like to express my earnest appreciation of my supervisors: Associate Professor Henrik Leion, Professor Tobias Mattisson, and Doctor Daofeng Mei. To Henrik, I really appreciate all the guidance, kindness, and encouragements that you have constantly showed to me; not the least all the discussion that we have had regarding our shared interests in many aspects. To Tobias, I have learned a lot from your persistence, ambition, and enthusiasm in research; these have been significant to me. Thank you for always challenging me to be the best version of myself. To Daofeng, I am genuinely thankful for every second you devoted for our discussions in research and even beyond that; your dedication has always inspired me. Furthermore, I would like to thank Carl Johan Linderholm for his assistance and priceless help during my first months as a PhD student.

I would like to acknowledge the European Union's Horizon 2020 as having funded the project CLARA (Chemical Looping Gasification for Sustainable Production of Biofuels) under grant agreement No 817841 and the Swedish Energy Agency for funding the project number 51430-1. It has been a privilege to work in these projects. I am also grateful for all other parties that have provided research materials and facilities for this work.

My gratitude goes out to all my co-authors and colleagues who made this work possible and even better than I ever thought. Many thanks to the co-authors: Duygu Yilmaz, Ivana Staničić, Amir Hassan Soleimanisalim, and Magnus Rydén; your contributions have been invaluable. My sincere appreciation to all my colleagues in Energy Technology and Environmental Inorganic Chemistry who have always supported and helped me in many ways possible, especially Xiaoyun, Nasrin, Mariane, Fredrik, Viktor, Felicia, Ivan, Tharun, Esraa, and Ulf. Special thanks to Emil from the Technical University of Denmark; I really enjoyed our conversation and discussion when you visited Chalmers.

For all my time in Sweden, I would not be still standing here without the sincere friendship and moral supports from Iqbaal, Faris, Angie, and Annisa; I am truly grateful to have known all of you. To my best friend, Albertus Adrian Sutanto, I treasure our friendship in the deepest way possible. Thank you for always being there for me; not only as a travel companion, but also as the closest friend ever to me.

Last but not least, I would not have made it without the everlasting supports from my family, particularly my late mom, a strong-wonderful woman whom I will forever love and miss, and my dearest siblings: Linda and Daniel. Big thanks to my cousin, Laura, for always motivating me. To dear Gracia, thank you for believing in and encouraging me continuously.

Victor Purnomo
Göteborg, April 2022

List of Publications

This thesis is based on the experimental studies reported in these papers

Paper I

Purnomo, V., Yilmaz, D., Leion, H., Mattisson, T. (2021)
Study of defluidization of iron- and manganese-based oxygen carriers under highly reducing conditions in a lab-scale fluidized-bed batch reactor
Fuel Processing Technology, 219, 106874

Paper II

Purnomo, V., Staničić, I., Mei, D., Soleimanisalim, A. H., Mattisson, T., Rydén, M., Leion, H.
Iron sand as a by-product-based oxygen carrier for chemical-looping processes
Submitted for publication

Paper III

Purnomo, V., Mei, D., Soleimanisalim, A. H., Mattisson, T., Leion, H.
The effect of oxygen carrier's mass conversion degree on char conversion and its implication for chemical-looping gasification
Submitted for publication

Contribution report

Paper I	Principal author, experimental works, characterization, parts of data interpretation, writing
Paper II	Principal author, experimental works, characterization, parts of data and model analysis, writing
Paper III	Principal author, experimental works, characterization, parts of data and model analysis, writing

Table of Contents

1. Introduction	1
1.1 Background	1
1.1.1 Carbon capture technologies	2
1.1.2 Chemical-looping and oxygen-carrier-aided combustion	3
1.1.3 Chemical-looping gasification.....	4
1.2 Objectives.....	5
1.3 Thesis outline	5
2. Use of oxygen carriers in chemical-looping processes	7
2.1 Ilmenite.....	8
2.2 Iron sand	8
2.3 LD slag	8
2.4 Tierga ore	9
2.5 Sibelco manganese ore (calcined)	9
2.6 Elwaleed B manganese ore	9
3. Experimental section	11
3.1 Fluidized bed batch reactor setup.....	11
3.2 Pressure monitoring.....	12
3.3 Materials.....	12
3.3.1 Oxygen carriers.....	12
3.3.2 Gases.....	13
3.3.3 Solid fuel.....	14
3.4 Experimental methods.....	15
3.4.1 General steps in a cycle in the batch fluidized bed reactor	15
3.4.2 Syngas conversion with various oxygen carriers	16
3.4.3 Oxygen carrier’s reactivity toward methane	16
3.4.4 Particle bed defluidization observation	17
3.4.5 Solid fuel reactivity investigation.....	18
3.4 Data evaluation.....	18
3.4.1 Gaseous fuel	18
3.4.2 Solid fuel.....	19
3.5 Char reactivity models	19
3.6 Oxygen carrier characterization	21
4. Results and discussion	23
4.1 Syngas conversion with various oxygen carriers	23
4.2 Oxygen carrier’s reactivity toward methane	24
4.3 Defluidization of oxygen carriers at high reduction degrees	25
4.4 The reactivity of solid fuel toward oxygen carriers	29
5. Conclusions	33
Abbreviations and Nomenclatures	35
References	37

1. Introduction

1.1 Background

Our society is currently facing multiple environmental issues caused by the current ways of energy production and consumption that releases greenhouse gases into the atmosphere. These gases keep heat from escaping from the earth, which is desired to sustain life on the planet. Nevertheless, the recent era of industrialization has caused an excessive accumulation of greenhouse gases in the atmosphere, which eventually contributed to global warming and many unprecedented environmental issues [1]. The internationally adopted Paris Agreement aims to keep the global temperature increase below 1.5 °C, yet none of the actions taken has been proven sufficient to fulfill this target [2]. Most of the feasible renewable concepts often require a need for a costly new technology [3]. At the same time, many individuals are trying to promote a sustainable lifestyle by reducing energy consumption and waste on an individual basis; while this is good, it is not sufficient to meet the global goals [4]. After all, simply minimizing an individual carbon footprint can be deemed ineffective to slowing down the global warming and the subsequent climate change.

One promising concept that can be an answer to this issue is using the negative emissions of carbon dioxide, also known as the carbon-negative process [5]. This does not necessarily imply a direct reabsorption of all the released greenhouse gases out from the atmosphere, but rather the use of biomass-based fuels in an energy conversion process that is able to avoid releasing carbon dioxide into the atmosphere. Contrary to fossil fuels which adds more carbon to the atmosphere when burned [6], biomasses naturally obtain their carbon content from the atmosphere; thus, a biomass conversion that releases carbon dioxide into the environment can be considered as a carbon-neutral process. This is because the emission alone does not change the net balance of the carbon content in the atmosphere. Subsequently, if this released carbon dioxide from the biomass conversion is captured, the process indirectly reduces the carbon content in the atmosphere; hence, it is called a carbon-negative process [7]. Figure 1.1 illustrates the difference between carbon-positive, carbon-neutral, and carbon-negative processes.

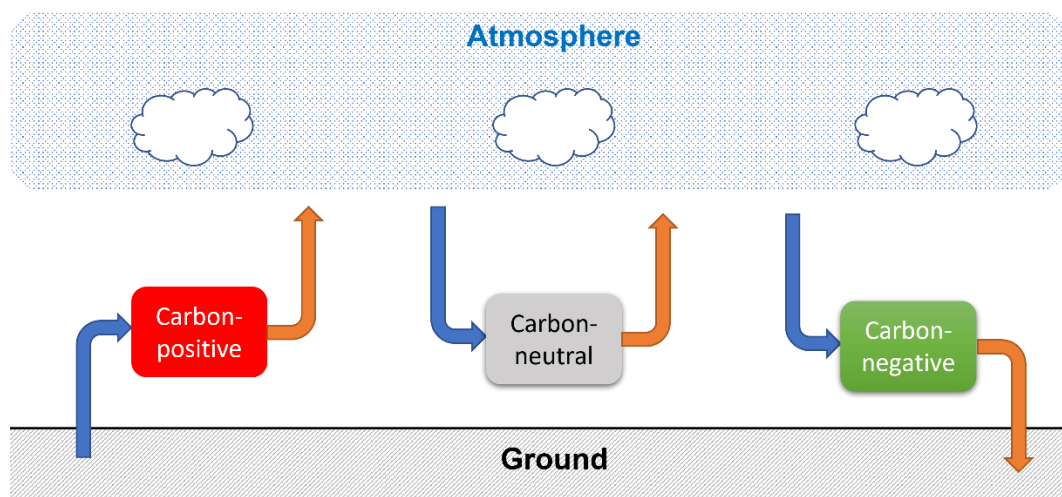


Figure 1.1. An illustration of carbon-positive, carbon-neutral, and carbon-negative processes, adapted from Matthews [7]. The blue and orange arrows indicate the flow of carbon sources and carbon emission, respectively.

1.1.1 Carbon capture technologies

The concept of carbon capture is the main feature of the carbon-negative process and has been recognized as a long-term solution to reduce the carbon emission into the atmosphere. According to a review by Osman et al [8], there are three main concepts in carbon capture: pre-combustion, post-combustion, and oxyfuel combustion routes. Adapted from a review article by Alalwan and Alminshid [9], Figure 1.2 below illustrates the difference between these concepts in an simplified way. The same article addressed both the advantages and disadvantages of each concept, which are summarized in Table 1.1. A common feature of all these processes is that they entail a form of gas separation step, which can be energy-intensive, implying a need for additional equipment.

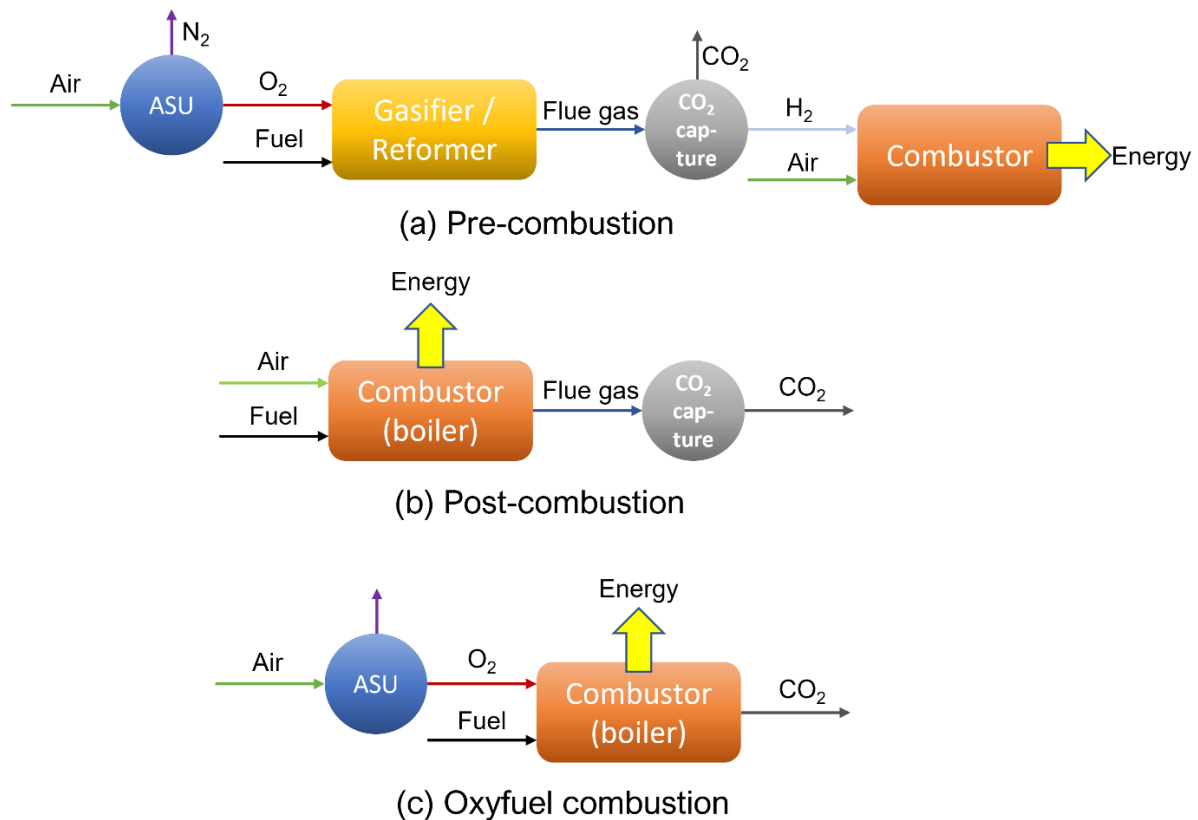


Figure 1.2 An over-simplified illustration of three carbon capture concepts, adapted from Alalwan and Alminshid [9]. ASU represents air separation unit.

Table 1.1 Advantages and disadvantages of three carbon capture concepts

Carbon capture concept	Advantages	Disadvantages
Pre-combustion	Simple CO ₂ separation, fair energy consumption, promoting H ₂ production	Additional purification steps may be required, which lower the energy efficiency and increase the running cost
Post-combustion	Already used commercially	Additional cost to generate electricity, energy-intensive CO ₂ capture
Oxyfuel combustion	High energy efficiency	Requires a large supply of pure oxygen

1.1.2 Chemical-looping and oxygen-carrier-aided combustion

Chemical-looping technology is sometimes seen as a second generation of oxyfuel combustion [10], yet others see it as a completely different concept and hence as the fourth concept of carbon capture [11]. To understand how chemical-looping technology has emerged as one of the most promising carbon-neutral processes, one needs to understand the unique arrangement of the technology. The most common setup involves two interconnected reactors where an oxygen carrier is circulated between the two reactors; namely air and fuel reactors, see Figure 1.3. An oxygen carrier (OC), usually a metal oxide, is oxidized in the air reactor (AR), and then circulated into the fuel reactor (FR), where it is reduced by fuel. The reduced OC is circulated back from the FR to the AR to complete the loop. This enables the fuel to react only with available oxygen carried by the OC without being mixed with any nitrogen, hence eliminating the need for an energy-intensive gas separation unit. If biomass is used as fuel in chemical-looping technology, the carbon balance can be improved even further to establish a carbon-negative process.

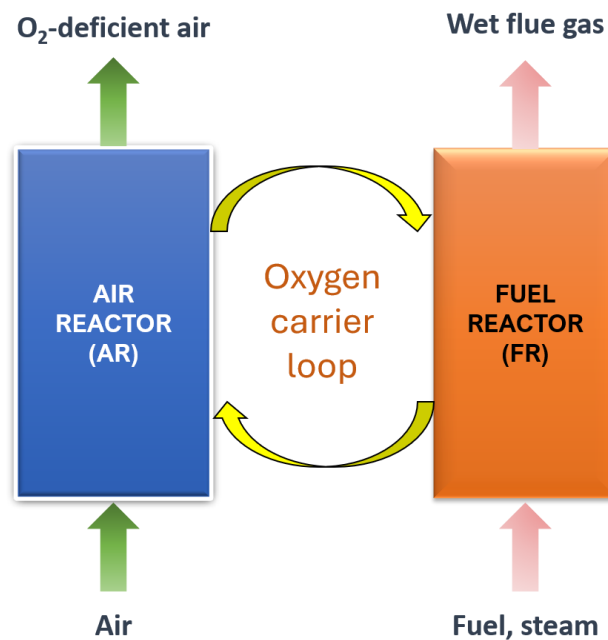


Figure 1.3 A general schematic diagram of the chemical-looping process. The circulating oxygen carrier is oxidized and reduced by fuel in the air and fuel reactors, respectively.

Another use of oxygen carriers is in the oxygen-carrier-aided combustion (OCAC), which uses the oxygen carrier as the bed material in a conventional fluidized bed boiler. Here, the oxygen carrier transports not only heat but also oxygen within the boiler. This will not capture any CO₂, but previous findings suggested that the use of an oxygen carrier in OCAC can reduce the emission levels and even enhance the combustion efficiency and capacity [12]. An OCAC boiler is illustrated in Figure 1.4.

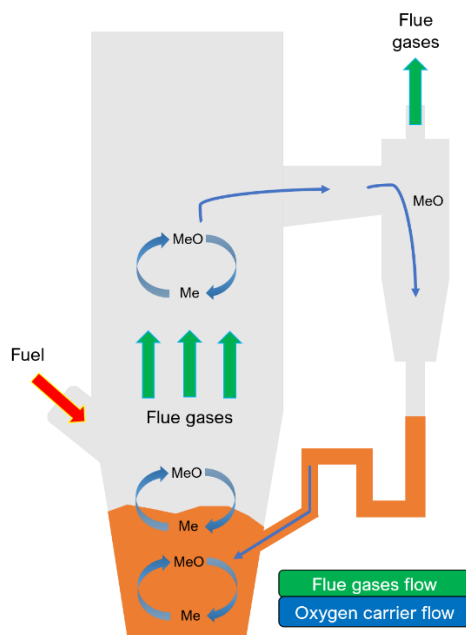


Figure 1.4 An illustration of an OCAC boiler. The oxygen carrier circulates between the upper and lower parts of the boiler and constantly experiences oxidation – reduction.

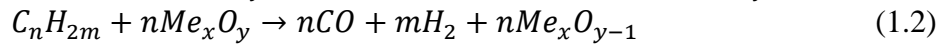
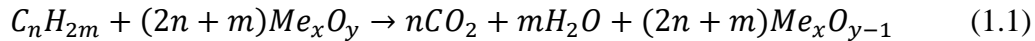
The oxidation of a reduced oxygen carrier, symbolized as “Me”, occurs in the dense bed (the orange-colored region) when the particles absorb oxygen upon contact with the bubble phase. The oxidized oxygen carrier, MeO, will later bring oxygen to oxidize CO and other volatile compounds in the emulsion phase or any part of the reactor, producing flue gases. This loop also happens in the splash zone and along the transport zone, yet to a lesser extent compared to that in the dense bed. This way, OCAC can overcome insufficient dispersion of air in the gas phase and incomplete fuel combustion [13].

It is clear that the oxygen carrier has an important role in both technologies mentioned above, which are nowadays emerging. Chemical-looping combustion has a low energy penalty compared to conventional energy conversions and is thus attractive in fulfilling environmentally sound energy demands. OCAC also provides a more environmentally friendly solution by facilitating a highly efficient combustion. Therefore, the need for extensive studies to characterize and screen oxygen carrier is essential. A more detailed elaboration on oxygen carriers is provided in Chapter 2.

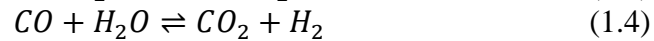
1.1.3 Chemical-looping gasification

Among many of the chemical-looping processes for solid fuels, chemical-looping gasification (CLG) is currently emerging. Instead of focusing on the heat and power generation like in chemical-looping combustion (CLC), CLG aims to produce valuable products like syngas that can be derived into many useful products through an extra synthesis process, for instance by a Fischer-Tropsch process. Chemical-looping reforming (CLR) is another process that has the same aim but uses gaseous fuels. In chemical-looping combustion (CLC), oxygen carriers are usually reduced by around 1% due to the high circulation of oxygen carriers to achieve the full oxidation of fuel. However, the desired product in CLG is CO and H₂, and the solid fuel should only be partially oxidized. Still, for an auto-thermal process, it is necessary to also produce CO₂ and H₂O in the fuel reactor, i.e., the outlet will be syngas containing mainly H₂, CO, as well as CO₂ and H₂O [14]. The main reactions that take place in the fuel reactor of CLC and CLG are illustrated in Equation (1.1) and (1.2), respectively. It should be noted that other

reactions, such as the water-gas shift reaction, may also take place; yet only these main reactions are shown here to point out the difference.



In CLG, the solid fuel conversion in the fuel reactor typically undergoes several steps. First, biomass is pyrolyzed into bioproducts. The intermediate pyrolysis products will then react with the oxygen carrier and reduce it. The consumption of the pyrolysis bioproducts will improve the pyrolysis itself, while CO₂ and H₂O produced from the reduction reaction act as gasifying agents that improve the biomass gasification [15]. The main steam gasification reaction is usually accompanied with the water-gas shift reaction [16]. The corresponding reactions are shown in Equation (1.3) and (1.4), respectively. Here, C represents the biomass char.



One way to maintain the partial oxidation of fuel is to limit the amount of available oxygen in the oxygen carrier from the air reactor to the fuel reactor. This can be performed by simply partially oxidizing the oxygen carrier in the air reactor; thus, the oxygen carrier is in a reduced state since it is not fully oxidized. However, this can lead to multiple performance issues of the oxygen carrier as an oxygen carrier in a reduced state may show lower reactivity, breakage, and possibly agglomerate or even defluidize. The tendency for these issues to occur in CLG vary between different oxygen carriers; thus, the works in this thesis focus on various oxygen carriers and how they performed in a fluidized bed setup under a highly reducing environment and high degree of solid reduction, something which has not previously been studied in detail.

1.2 Objectives

This thesis explores how a high reduction degree of oxygen carriers may affect their properties, which is relevant for CLG. These aspects could also be relevant for CLC, CLR, and OCAC where oxygen carriers could be reduced to further extents under certain conditions. The main focuses of this thesis are as follows:

- i) The reactivity of highly reduced oxygen carriers toward gaseous fuels
- ii) The fluidization performance of highly reduced oxygen carrier particles
- iii) The reactivity of a solid fuel char using highly reduced oxygen carriers

This thesis utilizes a combination of experimental works in a fluidized bed batch reactor and detailed physical and chemical analyses of solid materials. In this way, it is possible to gain a view of the important factors that determine the oxygen carrier's behavior at high degrees of reduction.

1.3 Thesis outline

This thesis is based on the papers mentioned in the list of publications. The background, objectives, and outline of this thesis are provided here in Chapter 1. Chapter 2 elaborates on the use of oxygen carriers, focusing on the principally studied materials in this thesis. Chapter 3 describes the materials and methodology used, and Chapter 4 discusses the results of the works conducted. Syngas conversion with these oxygen carriers is summarized (Paper I and II), followed by the reactivities of such materials toward methane (Paper I and II). The tendency for bed defluidization, observed in various highly reduced iron- and manganese-based oxygen carriers, is presented afterward (Paper I). Lastly, the reactivity of pine forest residue char using

ilmenite, the benchmark oxygen carrier, and iron sand, a new oxygen carrier candidate, are compared (Paper II and III). The fuel conversion inhibition caused by hydrogen, and the possible mechanisms causing it, are also presented in this section. Chapter 5 presents the main conclusions of this thesis.

2. Use of oxygen carriers in chemical-looping processes

Oxygen carriers are usually metal oxides that can absorb and transport oxygen. The use of oxygen carriers in these energy conversion processes has also been studied intensively and reviewed multiple times [17]–[19]. In chemical-looping technology, an oxygen carrier is used to enhance fuel conversion and achieve an inherent separation of gases. An oxygen carrier should be able to undergo multiple cycles of oxidation and reduction, making it possible to catch and release oxygen cyclically.

A good oxygen carrier should have the following characteristics: sufficiently reactive, highly durable, good fluidization performance, inexpensive, abundantly available, and environmentally safe. Certain oxygen carriers have been found to exhibit a unique characteristic known as chemical-looping oxygen uncoupling (CLOU), where they may release oxygen gas in the fuel reactor. This CLOU property is preferable since it can improve the reactivity between the oxygen carrier and fuels [20]. Many previous studies have investigated the characteristics of various oxygen carriers with different metal oxides. The general characteristics of the most studied oxygen carrier materials are summarized in Table 2.1.

Table 2.1 General characteristics of the most studied oxygen carrier materials

The base metal	Advantages	Disadvantages
Fe (iron)	Good stability and reactivity, environmentally friendly, abundantly available [17]	More prone to defluidization under highly reducing environment [21]
Mn (manganese)	Stable reactivity, possible CLOU properties, environmentally safe [22], [23]	Higher attrition rate compared to Fe-based oxygen carriers [24]
Ni (nickel)	High reactivity, high selectivity [25]	Expensive and toxic [26]
Cu (copper)	High reactivity, high oxygen transport capacity, CLOU properties [19]	Comparably costly, agglomeration problem [27]

Oxygen carriers can be either synthetically produced, naturally available, or obtained from a by-product or even waste material. Having been studied multiple times, the synthesized oxygen carriers in general show a better performance and require less efforts to characterize and modify [28], [29]. Nevertheless, these carefully engineered oxygen carriers take considerable effort to produce and are therefore costly, making a wider use of them in larger scale processes currently limited. Natural ores can be obtained easily, but they may experience a decrease in their reactivity over multiple reduction-oxidation cycles [30]. Moreover, they always contain impurities. Still, the use of natural minerals can be considered feasible as long as the lifetime is sufficient and no major defluidization or agglomeration problem is present. Materials obtained from by-products or industrial waste are economically attractive as oxygen carriers since the use of these materials can support a circular economy. Previous studies have found some promising results on the reactivity and performance of such materials [31], [32]. One essential characteristic that these materials should possess is that they contain no or very little toxic elements to minimize the environmental risks. Otherwise, an extra pretreatment will be required and may therefore incur extra costs.

When utilizing biomass as fuel, which contains significant fractions of reactive ash species, it is likely that natural ores or by-products will be the most suitable oxygen carrier materials. This is because interactions with ash species are inevitable and will consequently limit the residence time of the oxygen carriers; thus, the use of synthesized oxygen carriers is not economically and practically justifiable.

Below are short presentations for each oxygen carrier investigated in this thesis. The composition of the respective oxygen carriers will be provided in Chapter 3, more precisely in Table 3.1.

2.1 Ilmenite

Among the widely studied oxygen carriers, ilmenite is known as the benchmark oxygen carrier for both chemical-looping combustion (CLC) and OCAC since it has been successfully tested in multiple operations [33]–[36]. The ilmenite referred to in this thesis is not the pure ilmenite phase (FeTiO_3), but rather an iron-titanium mineral ore, which was in this case provided by Titania A/S in Norway. The ilmenite used in this work comprises around 34 wt.% Fe and 28 wt.% Ti [37]. Apart from being inexpensive and easily obtainable, ilmenite has in general shown a good reactivity toward CO and H_2 , yet lower reactivity toward methane [38], [39]. Despite this, ilmenite has shown a sufficient reactivity toward solid fuels in various operations [40].

2.2 Iron sand

Iron sand is a new iron-based oxygen carrier candidate that is investigated in this thesis (Paper II). The iron sand in this work is a by-product from a copper smelting plant run by Boliden AB in Rönnskär in Northern Sweden. The product is from the slag fuming process and was separated from the other products by a settling furnace. Previous studies used the name “copper slag” for the material [41]–[43], but the name “iron sand” was deemed to be more representative to reflect the material’s content, which actually contains very little copper. The reasonable amount of iron content in the material, nearly 35 wt.% Fe, is the main reason to consider this by-product as an oxygen carrier [18].

The proposed by-product-based material is attractive not only due to its low cost, but also its sufficient reactivity to convert both gaseous and solid fuels and reasonable fluidization performance, which was reported in Paper II. The results indicated that iron sand might have lower oxygen capacity compared to ilmenite, which means the amount of available oxygen that iron sand can carry to the fuel reactor is less than that of ilmenite. This makes iron sand more suitable for processes where oxygen transfer should be limited to maintain a partial oxidation of fuels, such as in chemical-looping gasification (CLG).

2.3 LD slag

Also known as a steel-converted slag, Linz-Donawitz (LD) slag is an iron-based by-product from the steel industry that also contains a significant content of calcium [44]. The material was provided by the Swedish steel production company SSAB and has been studied as an oxygen carrier in both laboratory and pilot scales [45], [46]. LD slag is usually produced in a massive quantity, which decreases its cost significantly. Its oxygen capacity is only around 1 wt.%, which is lower than ilmenite and therefore just like iron sand, making it interesting for processes such as CLG or CLR. The high calcium content in LD slag is interesting as CaO has been known for its ability to catalyze methane conversion [47], and LD slag itself has been

found to catalyze the water-gas shift reaction during fuel conversion [44]. LD slag can also be used to reform tars [48].

2.4 Tierga ore

Tierga ore is an iron-based mineral ore obtained from a hematite mine in Tierga, Spain. The material has been studied several times and Tierga ore show high reactivity particularly toward hydrogen [49]. It was also found previously that the CaO content (4.7 wt.%) in the material can to some extent absorb SO₂ [50]. The attrition of Tierga ore has been investigated in hot conditions [51]. Tierga ore has also been previously tested in a 1.5 kW biomass chemical-looping gasification (BCLG) unit [24].

2.5 Sibelco manganese ore (calcined)

This manganese ore was sourced from Sibelco Nordic AB in a calcined form. The material is notable for its CLOU properties and high reactivity toward syngas [22]. Another study, however, found that calcined Sibelco showed a low reactivity toward methane, but it has a reasonable physical durability [52]. The material has been investigated in both 10 and 100-kW chemical-looping combustion units [53], [54].

2.6 Elwaleed B manganese ore

Elwaleed Grade B is an Egyptian manganese ore with higher iron content compared to Sibelco (calcined). The material has CLOU properties and a previous study suggested that Elwaleed B had a higher reactivity toward methane compared to Sibelco (calcined) [52]. The reactivity of the material in a 10-kW pilot rig was found to be higher than that of ilmenite and its lifetime is similar to that of ilmenite [55].

3. Experimental section

3.1 Fluidized bed batch reactor setup

The fluidized bed batch reactor setup is illustrated in Figure 3.1 below. Batch means that the operation is non-continuous; thus, a series of steps is involved.

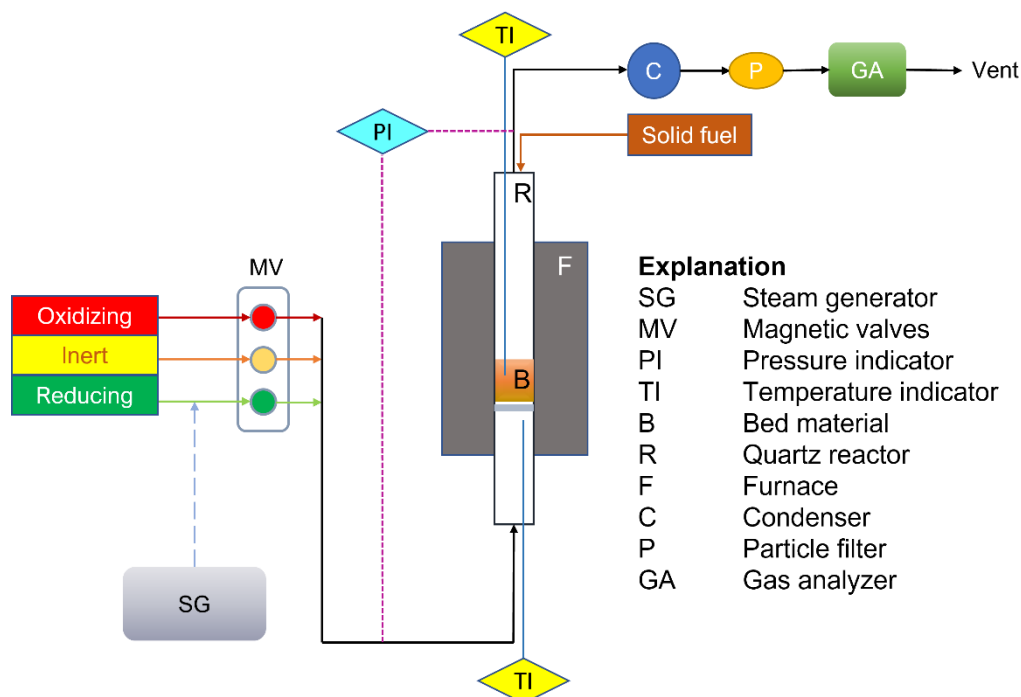


Figure 3.1 A schematic setup of the fluidized bed batch reactor system

The same type of reactor was used for both solid and gaseous fuel experiments, although the way of feeding fuel was different. The feeding of gases was regulated by three magnetic valves. Solid fuel was fed into the reactor from the top, while either steam or gaseous fuel was fed through the bottom during the reduction phase. The height and inner diameter of the quartz glass reactor was 820 mm and 22 mm, respectively. The bed particles were placed on top of a porous circle-shaped quartz plate, which was located 370 mm above the reactor's bottom edge. The reactor was placed in a high-temperature furnace manufactured by ElectroHeat Sweden AB. The inlet and outlet of the reactor were equipped with tight-sealed connections to avoid gas leakage. A heating tape was wrapped around the reactor's top to avoid the condensation of gas, particularly water vapor, in this area. In the case with tests involving solid fuel, an additional heating tape was installed around the bottom of the reactor to avoid steam condensation. Sweep gas, which was nitrogen, was introduced from the top of the reactor to assist the feeding of solid fuels. It should be noted that the sweep gas did not reach the particle bed due to its relatively low velocity, which was no more than half of the fluidizing velocity, and therefore did not affect the fuel conversion in the bed itself. The temperature inside the bed of particles was measured using a type-K thermocouple that was placed in a quartz cover. The outlet gases were cooled down by an M&C ECP1000 cooler before entering the analyzer; thereby removing the water contents. A Rosemount™ NGA 2000 gas analyzer measured the real-time gas volumetric flow rates and concentration. The steam used as fluidizing gas was generated by the controlled evaporator mixer Bronkhorst type W-202A-300-K. The pressure monitoring setup will be discussed in sub-chapter 3.2.

3.2 Pressure monitoring

To monitor the fluidization of the bed particle, a 20-Hz Honeywell pressure transducer was employed to measure the pressure difference between the inlet and outlet of the reactor. Despite its small frequency, the pressure transducer worked very well to judge the bed fluidization in this small system. When defluidization occurs, the pressure difference will drop significantly in the pressure monitor. This is illustrated in Figure 3.2.

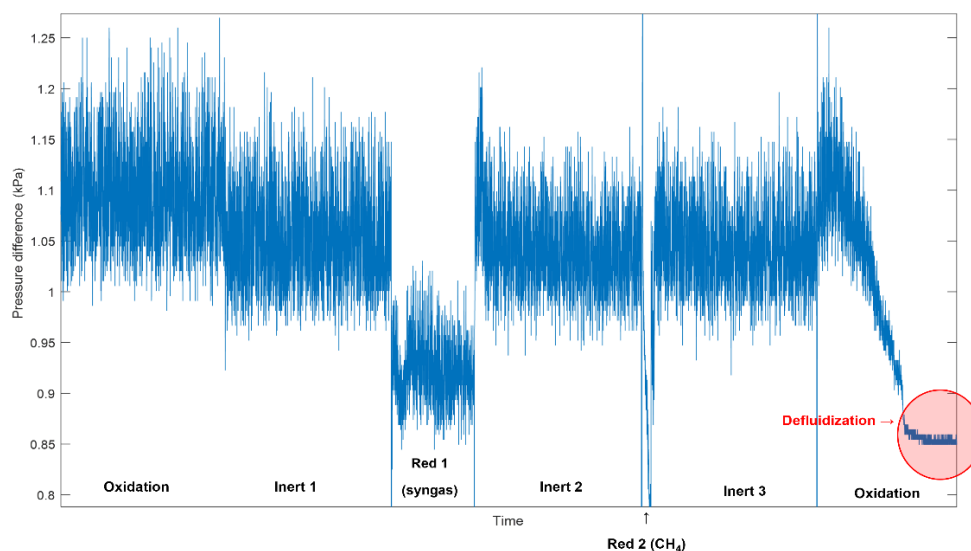


Figure 3.2 Defluidization detected in the bed based on the sudden decrease in pressure fluctuations during oxidation. In this case, the OC was ilmenite tested at 900 °C, and defluidization happened during the oxidation that followed a 90-second syngas reduction, which corresponds to a reduction of around 3% ($\omega = 97\%$). The frequency of pressure measurement was 20 Hz.

Here, the bed defluidization is indicated by a change in the pressure fluctuation, which suddenly became substantially low. However, not all sudden drops in the pressure fluctuations indicate a defluidized bed. For example, the sudden drop between oxidation and inert 1 or even inert 1 and reduction 1 in the graph was due to different flow rates and changes in flow streams. A simple test in cold condition showed that the bed can be deemed fluidizing when the standard deviation (SD) of pressure fluctuations was at least around 0.02 kPa. Thus, as long as the SD of the pressure fluctuations exceeds this threshold, the bed still fluidized. The SD ranged between 0.03 – 0.06 kPa during the whole experiments in hot situations when the bed fluidized. The SD is simply used to judge the fluidization state of the bed based on pressure fluctuations and does not necessarily indicate the absolute pressure in the bed.

3.3 Materials

3.3.1 Oxygen carriers

All oxygen carriers in this work were prepared according to Figure 3.3. All materials are naturally obtained or by-product-based and often received in suitable size ranges. Still, it was deemed necessary to heat treat and sieve the materials prior to use in order to have a common basis for comparison. The calcination of oxygen carriers was performed to remove moisture and organic impurities in the oxygen carrier, as well as to strengthen the particle's structure

[16]. Sieving the calcined oxygen carrier was necessary since choosing a suitable particle size range is important to ensure a good fluidization performance. Activation of the oxygen carrier bed aimed to prepare the oxygen carrier through several oxidation – reduction cycles at a lower temperature, e.g., 850 °C in this case, which may contribute to a more stable reactivity and a lower risk for an early bed defluidization [47], [56]. The reduction was performed using syngas as the oxygen carriers usually have reasonable reactivity toward syngas.

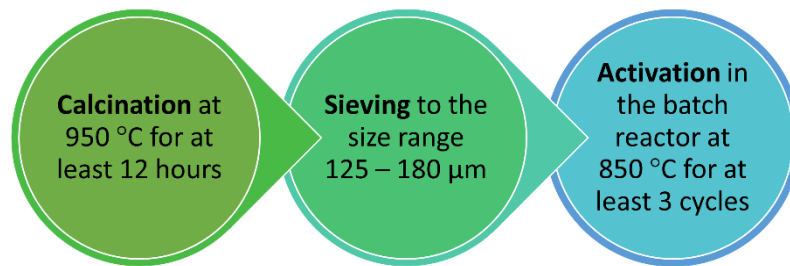


Figure 3.3 Steps in oxygen carrier preparation

Various oxygen iron- and manganese-based oxygen carriers have been investigated. Table 3.1 shows the main elemental composition of all the oxygen carriers used in this thesis. It should be noted that the oxygen content, the combustible parts, and the constituents are not included in the table; this is why the totals do not reach 100%. It can be seen that ilmenite and Tierga ore as iron ores have more than 50 wt.% Fe; while iron sand and LD slag as by-products have lower iron contents, between 20 – 40 wt.% Fe. Apart from their manganese content, Sibelco (calcined) and Elwaleed B also have minor contents of iron.

Table 3.1 Main elemental composition of oxygen carriers used in this thesis

Element	Composition (wt.%)					
	Ilmenite	Iron sand	LD slag	Tierga ore	Sibelco (calcined)	Elwaleed B
Fe	34	35	24	52	5.2	22
Mn	0.48	0.35	3.6	0.04	46	32
Si	0.15	16	10	3.4	3.7	4.7
Ti	28	0.13	1.1	0.08	0.23	0.08
Ca	0.06	2.3	49.5	2	2	1.7
Al	0.19	2.4	1.3	1.7	3.4	1.2

3.3.2 Gases

The gases used in this work are common gases that are present in most combustion or gasification processes. Table 3.2 provides a summary of gases used in this thesis. Syngas, methane, and diluted CO are reducing gases and can be considered as gaseous fuels. These gases were used as they are components of biomass volatiles. The oxygen content in the oxidizing gas was limited to 5%, instead of around 21% in normal air, since this is the target oxygen concentration in the outgoing gas at the top of the riser of a chemical-looping combustion unit [57], [58]. Given that an oxygen carrier should be able to be oxidized at lower partial pressures of oxygen in order to be deemed feasible, using this concentration is reasonable. Additionally, using a low concentration of oxygen is needed to avoid excessive heating during the exothermic oxidation step [59].

Table 3.2 Gases used in this thesis

Gases	Composition
Oxidizing gas	5% O ₂ , 95% N ₂
Nitrogen	100% N ₂
Syngas	50% CO, 50% H ₂
Methane	100% CH ₄
Diluted CO	50% CO, 50% N ₂

3.3.3 Solid fuel

In this thesis, there was only one solid fuel used, namely pine forest residue char. The fuel was obtained from Navarra, Northern Spain [60]. The char was prepared according to Figure 3.4 prior to being exposed to the solid fuel reactivity tests. Using the raw fuel directly in the experiments was deemed not feasible as the material in its original form tend to stick to the inner surface of the feeding line.

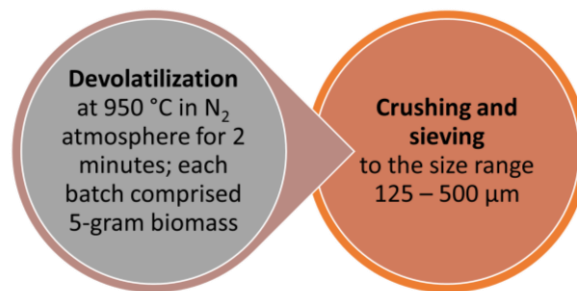


Figure 3.4 Steps in solid fuel preparation

Devolatilization was considered an important step with aims to remove major volatile contents in the fuel that may disturb product gas concentration measurement or even suppress the char reactivity [61]. Crushing and sieving were necessary to acquire a suitable size range of solid fuel; otherwise, the fuel feeding into the batch reactor would have been challenging. If the fuel is too fine, it might stick to the inner surface of the feeder and not get into the reactor. On the other hand, if the fuel is too coarse, it might become stuck within the feeders. In the experiment using solid fuel, nitrogen and steam were also present in the bed to facilitate the fluidization and gasification, respectively. The composition of pine forest residue char is provided in Table 3.3; the composition of oxygen is excluded here. The small moisture content in the char could be caused by water content in the air that was absorbed by the char during its storage prior to the fuel analysis.

Table 3.3 The composition of pine forest residue char

Element	Content (wt.%)
Total moisture	5.3
Ash	14.1
Chlorine (Cl)	0.01
Sulfur (S)	0.05
Carbon (C)	75
Hydrogen (H)	1.1
Nitrogen (N)	0.4
Ash element	Content (wt.% dry)
Aluminum (Al)	0.45
Silicon (Si)	1.90
Iron (Fe)	3.90
Titanium (Ti)	0.18
Manganese (Mn)	0.22
Magnesium (Mg)	0.31
Calcium (Ca)	1.90
Barium (Ba)	0.03
Sodium (Na)	0.07
Potassium (K)	0.63
Phosphor (P)	0.10

3.4 Experimental methods

The methodology for the experiments varied depending upon the goal and aim of the particular study; for details, see the appended papers.

3.4.1 General steps in a cycle in the batch fluidized bed reactor

A cycle in the fluidized bed batch experiment has three main steps. This is illustrated in Figure 3.5.



Figure 3.5 Three steps in a cycle in the fluidized bed batch reactor experiment

Normally, a cycle starts with the oxidation, where the oxygen carrier is oxidized with 5% O₂ in N₂, and then followed by an inert period, where nitrogen is used to purge the remaining oxygen in the system. During the reduction, either a solid fuel with steam or gaseous fuel is injected into the bed, and this will be followed by another inert period to purge flue gases. The next step can be either oxidation, which marks the beginning of a new cycle, or another reduction step, depending on the experimental plan. For example, many cycles in this thesis involved two steps of reduction in a single cycle, thus the sequence in the cycle was oxidation – inert – reduction 1 – inert – reduction 2 – inert.

3.4.2 Syngas conversion with various oxygen carriers

The syngas conversion with respect to various oxygen carriers compared here was adapted from both Paper I and II. The experiments were carried out by reducing fully oxidized oxygen carriers with syngas for certain periods. To maintain a simple comparison, only fresh-calcined materials will be compared here at their longest syngas reduction period. Several used materials were also investigated, see Paper I. Here the used materials were ilmenite, LD slag, Sibelco (calcined) and Elwaleed B. All experiments were conducted at 900 °C. Table 3.4 shows the summary of the longest length of reduction for syngas conversion that is being discussed in this thesis.

Table 3.4 The longest reduction length for syngas conversion with various fresh-calcined oxygen carriers at 900 °C. The flow rate of syngas was 600 ml/min.

Material	The longest length of reduction with syngas (s)	Corresponding paper
Ilmenite	90	I
Tierga ore	160	I
LD slag	40	I
Sibelco (calcined)	60	I
Elwaleed B	120	I
Iron sand	40	II

The reason behind different syngas reduction durations for different materials in Paper I was that the tests aimed to observe how far the oxygen carriers could be reduced until they defluidized. Subsequently, the duration was increased gradually until defluidization occurred. Several materials did not defluidize at all despite high reduction levels. In this case, the experiment was stopped when syngas conversion already became substantially low even though the bed still fluidized.

In Paper II, iron sand was reduced with syngas followed by pulses of methane. The central interest for this examination was not on the syngas conversion itself, but rather on the material's reactivity toward methane pulse. However, this material was not tested in Paper I; thus, it would still be interesting to compare the syngas conversions obtained in Paper I with that of iron sand in Paper II.

3.4.3 Oxygen carrier's reactivity toward methane

The reactivity of oxygen carrier toward methane was observed in slightly different procedures in two different articles (Paper I and II); yet principally, methane was fed to the bed particles in pulses. Pulsing of methane was performed to minimize the back mixing phenomenon, which can disturb the reactivity investigation. Similar to the procedure in sub-section 3.4.2, only fresh materials tested at 900 °C are discussed in this thesis. All methane pulses were introduced after a certain period of reduction with syngas. The motivation for determining the reactivity of oxygen carriers toward methane in addition to syngas is that the reactivity may differ with different gaseous fuels. Furthermore, both syngas and methane are components of biomass volatiles. Table 3.5 summarizes the difference in the way of pulsing methane to the particle bed in different papers.

Table 3.5 Two different ways of pulsing methane to the particle bed at 900 °C. Methane was always pulsed after the syngas reduction period with an inert step in between.

Material	Procedure of methane injection	Corresponding paper	Flow rate of methane (ml/min)
Ilmenite	A single 10-second methane pulse	I	450
Tierga ore		I	450
LD slag		I	450
Sibelco (calcined)		I	450
Elwaleed B		I	450
Iron sand	Ten 4-second methane pulses, with an inert step in between	II	600

3.4.4 Particle bed defluidization observation

Defluidization tendencies were gauged in all fluidized bed experiments in all appended papers, but Paper I had a specific aim of determining the defluidization tendency of oxygen carriers at high reduction degrees in gaseous environments. The specific defluidization tendency investigation was generally conducted according to Figure 3.6. The number of cycles and reduction length with syngas are provided in Paper I. The reaction temperature was set to 900 °C under atmospheric pressure. The sample abbreviations are provided in Table 3.6.

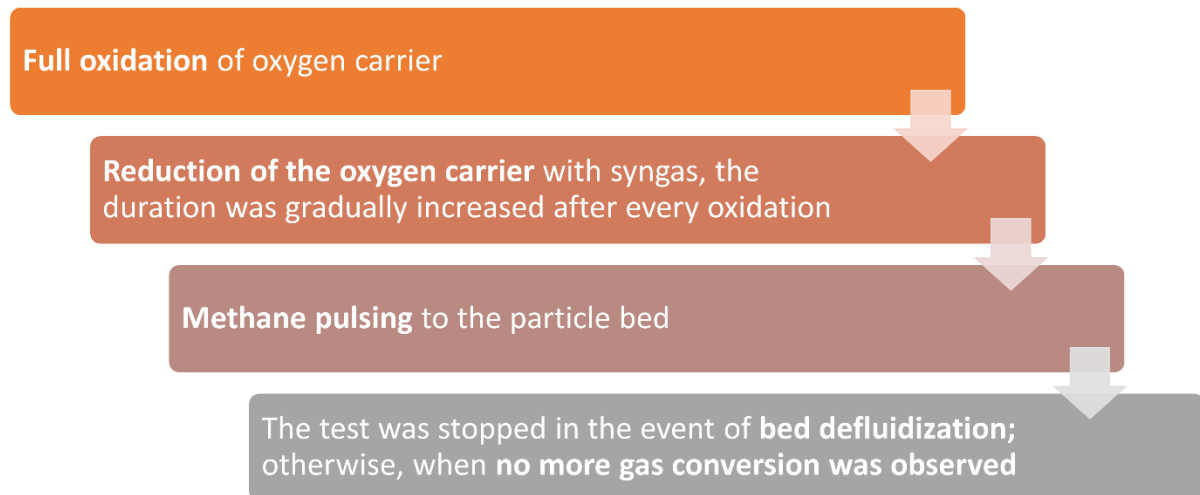


Figure 3.6 The simplified procedure for defluidization observation

3.4.5 Solid fuel reactivity investigation

The solid fuel reactivity tests were performed with one fuel, pine forest residue char, and two different oxygen carriers, namely iron sand (Paper II) and ilmenite (Paper III). The testing procedure for both oxygen carriers was the same and is summarized in Figure 3.7.

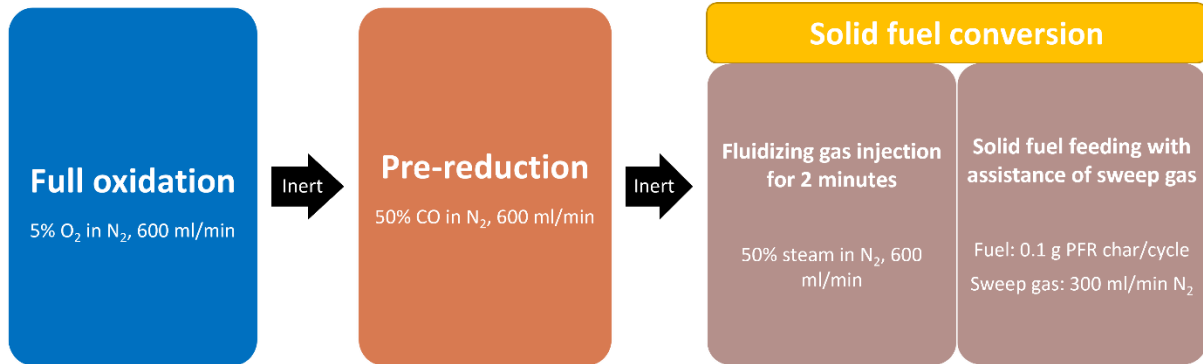


Figure 3.7 The simplified procedure of solid fuel reactivity tests using both iron sand and ilmenite as oxygen carriers. An inert gas, 600 ml/min of nitrogen was introduced between all phases to purge the remaining gases.

3.4 Data evaluation

3.4.1 Gaseous fuel

The mass conversion degree ω of the oxygen carrier under reduction with several gaseous fuels is calculated based on equations listed in Table 3.6. Here, x , \dot{n} , and M indicate mol fraction, molar gas flow, and molecular weight, respectively.

Table 3.6 Formula to calculate the mass conversion degree of the oxygen carrier upon reduction by various gaseous fuels

Gaseous fuel	Formula to calculate mass conversion degree	Equation number
Syngas	$\omega_{i,syngas} = \omega_{i-1} - \int_{t_{i-1}}^{t_i} \frac{\dot{n} M_O}{m_{ox}} (2x_{CO_2} + x_{CO} - x_{H_2}) dt$	(3.1)
Methane	$\omega_{i,CH_4} = \omega_{i-1} - \int_{t_{i-1}}^{t_i} \frac{\dot{n} M_O}{m_{ox}} (4x_{CO_2} + 3x_{CO} - x_{H_2}) dt$	(3.2)
Diluted CO	$\omega_{i,CO} = \omega_{i-1} - \int_{t_{i-1}}^{t_i} \frac{\dot{n} M_O}{m_{ox}} (x_{CO_2}) dt$	(3.3)

The yield of a carbon-based gas species i (γ_i) was defined as the mol fraction of gas species i divided by the total mol fraction of the carbon-based gases measured in the outlet. These include CO_2 , CO , and CH_4 , as they are the only three gases that the gas analyzers can possibly detect.

$$\gamma_i = \frac{x_i}{x_{CO_2} + x_{CO} + x_{CH_4}} \quad (3.4)$$

In this thesis, the conversion rate for gaseous fuels r was defined as the change of mass conversion degree within a certain period of time.

$$r = \frac{-d\omega}{dt} \quad (3.5)$$

3.4.2 Solid fuel

The fraction of converted carbon, X_c , was defined as the total carbon released during a specific time divided by the total carbon emitted from the converted char, $m_{c,total}$, during the conversion period.

$$X_c = \frac{M_c \int_{t_0}^t \dot{n}(t) (x_{CO}(t) + x_{CO_2}(t) + x_{CH_4}(t)) dt}{m_{c,total}} \quad (3.6)$$

Meanwhile, the conversion rate was defined as a function of X_c as shown in Equation (3.7) below.

$$r = \frac{dX_c}{(1-X_c) dt} \quad (3.7)$$

It should be noted that the conversion rate in this work was calculated within the range $0.3 < X_c < 0.7$, as this has been deemed the suitable range where the conversion rates are more stable based on previous tests in the same setup [62]. At a fraction of converted carbon lower than 0.3, the conversion rate could have shown an overshoot due to the volatile release in the beginning of the char conversion. The rate in a fraction of converted carbon higher than 0.7 may be overestimated due to the very low amount of fuel in the bed combined with low outlet flue gas concentration, which means that the denominator in Equation (3.7) becomes very low and the rate calculation will thus not be reliable.

3.5 Char reactivity models

The char reactivity with different oxygen carriers was compared in this work. As the first step, the Arrhenius equation in Equation (3.8) can give information on the rate constant k and activation energy E_a .

$$r = k e^{-\frac{E_a}{RT}} \quad (3.8)$$

R is the gas universal constant and T is the absolute temperature.

The equation above can be derived to Equation (3.9) below, which is the basis for the Arrhenius plot.

$$\ln(r) = \ln(k) - \frac{E_a}{RT} \quad (3.9)$$

The Arrhenius plot was made by plotting the natural logarithmic of char conversion rate r , obtained from Equation (3.7), as a function of the inverse of temperature, $1/T$. The rate constant k and activation energy E_a could be calculated from the intercept $\ln(k)$ and the slope $-E_a/R$, respectively.

The char conversion rate can be suppressed by the presence of both hydrogen and carbon monoxide [63]. In steam char conversion, the inhibition effect caused by hydrogen partial pressure has been found to be more important than that of carbon monoxide, which is usually more relevant for CO_2 gasification [62]. A high concentration of hydrogen has been found to significantly suppress the char conversion rate [64]. The proposed main mechanisms taking place in a steam char conversion are summarized in Table 3.7. These mechanisms have been previously found to be suitable to interpret steam char conversion, where a mixture of steam,

CO, CO₂, and CH₄ is involved [65][66]. C_f represents a free active site on the char's surface and C(X)_n denotes a char's surface complex which adsorbs n molecules of species X.

Table 3.7 The Langmuir – Hinshelwood mechanisms which have been explored in this work

Mechanism	Reaction	Equation number	Inhibition occurrence
Oxygen exchange (OE)	$C_f + H_2O \xrightleftharpoons[k_{-1}]{k_1} C(O) + H_2$	(3.10) (3.11)	If more hydrogen is added, the formation of C(O) may be suppressed (reverse of Equation 10)
	$C(O) \xrightarrow{k_2} CO + C_f$		
Associative hydrogen adsorption (AHA)	$C_f + H_2 \xrightleftharpoons[k_{-3}]{k_3} C(H)_2$	(3.12)	The added hydrogen is adsorbed directly onto the active sites from the gas phases according to either Equation (3.12) or (3.13)
Dissociative hydrogen adsorption (DHA)	$C_f + \frac{1}{2}H_2 \xrightleftharpoons[k_{-4}]{k_4} C(H)$	(3.13)	

The hydrogen inhibition mechanisms can be translated into three conversion rate models, which are all based on the general surface rate equation below, known as the Langmuir – Hinshelwood rate expression [66].

$$r = \frac{ck_1p_{H_2O}}{1 + \frac{k_1}{k_2}p_{H_2O} + f(p_{H_2})} \quad (3.14)$$

Functions of hydrogen partial pressure, here represented as $f(p_{H_2})$, is the factor that makes a difference between the three mechanism models. The following forms have been investigated in this thesis.

$$\text{OE: } f(p_{H_2}) = \frac{k_{-1}}{k_2} p_{H_2}$$

$$\text{AHA: } f(p_{H_2}) = \frac{k_3}{k_{-3}} p_{H_2}$$

$$\text{DHA: } f(p_{H_2}) = \frac{k_4}{k_{-4}} p_{H_2}^{0.5}$$

The models can later be simplified to make the validation easier, as can be seen in Table 3.8. Here, p_{H_2O} is the partial pressure of steam, which was assumed to be constant at 0.5 atm during all the experiments.

Table 3.8 The simplified formula for the Langmuir – Hinshelwood models to interpret steam char conversion

Mechanism	Simplified mechanism model	Parameter a	Parameter b
Oxygen exchange (OE)	$r = \frac{1}{a + bpH_2}$	$a = \frac{1}{c_f k_1 p H_2 O} + \frac{1}{c k_2}$	$b = \frac{k_{-1}}{k_2 c_f k_1 p H_2 O}$
Associative hydrogen adsorption (AHA)			$b = \frac{k_3}{k_{-3} c_f k_1 p H_2 O}$
Dissociative hydrogen adsorption (DHA)	$r = \frac{1}{a + b\sqrt{pH_2}}$		$b = \frac{k_4}{k_{-4} c_f k_1 p H_2 O}$

By plotting $1/r$ against the hydrogen partial pressure, the parameters a and b were obtained, and the mechanism taking place during the char conversion could be assessed. It can be seen that the OE and AHA models share the same equation structure; the only difference is what the parameter b stands for. The DHA model, on the other hand, has a different reaction order with respect to hydrogen partial pressure.

3.6 Oxygen carrier characterization

The crystalline phases of oxygen carrier samples were analyzed using either XRD Bruker D8 Advance or XRD Bruker D8 Discover. The analysis took roughly an hour for each sample with at least 800 steps using a copper radiation source. This was done to see how the phases of oxygen carriers might have transformed during the experiment. The surface morphology and elemental distribution in the oxygen carrier were analyzed using SEM/EDX JEOL 7800F Prime using a backscattered electron detector with an acceleration voltage between 10 to 15 kV. The oxygen carrier particles were embedded in epoxy and polished to provide a cross-sectional view under EDX. From this analysis, one can visualize the structural changes that the oxygen carriers had undergone during experiments. The defluidized oxygen carriers were observed under the light microscope Nikon SMZ800 to see what the particles looked like after the experiments., e.g. how the agglomerated particles were attached to each other.

4. Results and discussion

4.1 Syngas conversion with various oxygen carriers

Comprising high fractions of carbon monoxide and hydrogen, syngas is an important gas in chemical-looping processes. The gasification of char taking place in the fuel reactor will primarily produce CO and H₂ [67]; these gases make up a large part of the fuel volatiles. Evaluating syngas conversion with different oxygen carrier materials can give a basic insight into the oxygen carrier's suitability in CLG as well as the potential of CO and H₂ generation from the process. The CO₂ gas yield from the syngas conversion during the last cycle, i.e., when the syngas reduction period was the longest (see Table 3.4) for fresh materials, is compared in Figure 4.1 for all oxygen carriers used in this work. In this thesis, syngas constitutes of 50% CO and 50% H₂, but only the CO part can be evaluated by the CO₂ gas yield. Nonetheless, H₂ is known to have a higher reactivity than CO [47].

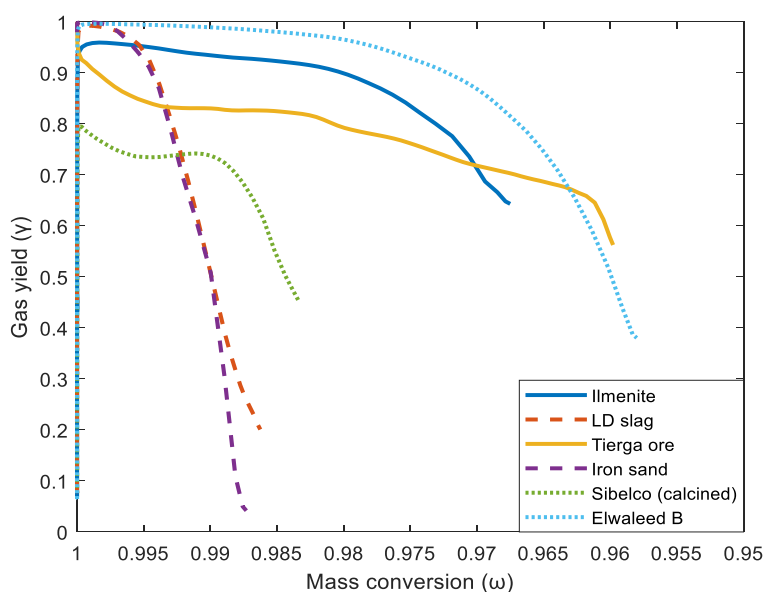


Figure 4.1 The CO₂ gas yield from the conversion of syngas for each fresh oxygen carrier material at the longest reduction period at 900 °C. The solid, dashed, and dotted lines indicate the iron ores, iron-based by-product materials, and manganese ores; respectively.

All materials exhibited a high syngas conversion to CO₂ of more than 90% in a fully oxidized state, except Sibelco (calcined). Still, the latter material showed a syngas conversion of around 80% at this state.

The iron ores, ilmenite and Ti erga ore, experienced a slow decrease in the syngas conversion, still remained high (above 55%) even at higher reduction degrees ($\Delta\omega > 3\%$). On the other hand, the iron-based by-product materials showed a rapid decline in the syngas conversion, which was already lower than 20% at $\Delta\omega \geq 1.25\%$. The rapidly declining trends were close to each other for both LD slag and iron sand; this could be caused by their lower iron content compared to that of the iron ores. Even though by-product materials, which are in slag forms in this thesis, are attractive due to their low cost and high circular economic value, a sufficiently high syngas conversion might only take place at high oxidation degrees ($\omega > 99\%$). Since these slags do not have a high oxygen capacity the oxygen content is usually already exhausted at the mass conversion degree of around 99%. The materials are hence suitable in operations such

as CLG or CLR, where the available oxygen should be limited to maintain partial oxidation of fuel.

The manganese ores showed wildly different syngas conversion levels; thus, a common conclusion for the two manganese ores cannot be made. This may not be so strange as the manganese ores in this work have a notably different compositions, see Table 3.1. Despite this, it can be said that Elwaleed B clearly showed a more sustained syngas conversion even at a higher reduction degree (more than 90% at $\Delta\omega$ nearly 3%) compared to the calcined Sibelco. This could have been caused by the higher iron content of the former, which can contribute to a higher reactivity toward syngas. Compared to the slags, the oxygen capacity of both manganese ores can be expected to be higher. Both materials still showed a CO₂ gas yield of more than 70% even at higher reduction degrees, i.e., at mass conversion degrees of around 0.9875 and 0.965 for Sibelco (calcined) and Elwaleed B, respectively. All in all, these two manganese ores have a reasonable reactivity toward syngas even at higher reduction degrees.

4.2 Oxygen carrier's reactivity toward methane

Methane is an important gas since it is generated during the devolatilization of biomass. Since methane in the experiments was pulsed after a certain period of syngas reduction, the reactivity of oxygen carriers toward methane can be obtained at certain oxygen carrier reduction degrees. This is plotted in Figure 4.2 for every oxygen carriers' mass conversion degree that was set by the syngas reduction, see Paper I for more details. For iron sand, the data plotted was taken from the first of the ten pulses that followed the preceding syngas reduction, see a more detailed explanation in Paper II. The gas yield here was obtained from the integration of the corresponding gas released and the mass conversion degree was taken as the median value of the pulse.

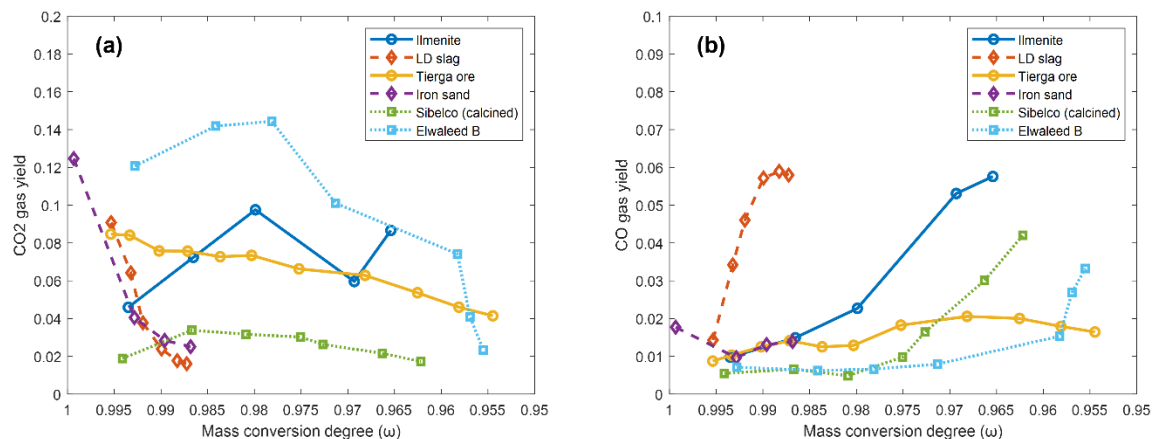


Figure 4.2 The gas yield of (a) CO₂ and (b) CO released from the conversion of methane at 900 °C with various oxygen carriers plotted as a function of mass conversion degree. Each dot represents a methane pulse that was injected to the bed after the period of syngas reduction. The solid, dashed, and dotted lines indicate the iron ores, iron-based by-product materials, and manganese ores; respectively.

In general, the gas yield of CO₂ tended to decrease at higher reduction degrees of the oxygen carriers. This increasing CO₂ gas yield of ilmenite after 3% reduction ($\omega = 97\%$) could have been partly caused by the formation of elemental iron, which is known for its ability to catalyze methane conversion at temperatures above 600 °C [68], at high reduction degrees. Still, the gas yield at this stage is quite low (less than 0.1); therefore, the increase itself does not necessarily imply that reducing ilmenite further could substantially improve methane conversion. The gas

yield of Sibelco (calcined) can be deemed as stable; the gas yield was low independent of the mass conversion degrees. Iron sand and LD slag, both being industrial by-product slags, showed a rapid decrease of the CO₂ gas yield; this is likely due to the low oxygen capacity, as discussed above.

The CO gas yield generally showed an increasing trend for all materials, except for the apparently stable CO gas yield of Tierga ore and iron sand. The available oxygen become more exhausted under a highly reducing environment; thus, the conversion of methane to CO is preferable. The Mn-based ores interestingly showed a rapid CO increase at lower mass conversion degrees ($\omega < 97.5\%$); this could have been caused by the rapid exhausting of the available oxygen in both oxygen carriers. Comparing the two by-product-based materials, LD slag released nearly 3 times as much CO as that released by iron sand from methane conversion at mass conversion degrees of less than 99%. CO released from methane conversion at around 1%-reduced LD slag is at a comparable level with that of 3.5%-reduced ilmenite. This suggested that LD slag would probably serve as a more suitable material to generate CO from CLG without a need to reduce the material to substantially lower mass conversion degrees.

4.3 Defluidization of oxygen carriers at high reduction degrees

In this thesis, considerable effort has been placed on the evaluation of the defluidization tendency of a number of materials. The summary of the results is provided in Table 4.1 below.

Table 4.1 Defluidization occurrence of the oxygen carriers

Base metal	Oxygen carrier			Was defluidization observed?	$\Delta\omega$ (%)	
	Name	State	Abbreviation		When defluidization was observed	When the outlet concentration of CO was equal to CO ₂
Fe	Ilmenite	Fresh-calcined	ILFC	Yes	3.2	-
		After-used	ILAU	Yes	3.7	-
	Tierga ore	Fresh-calcined	TOFC	Yes	4.0	-
	LD slag	Fresh-calcined	LDFC	No	-	0.9
		After-used	LDAU	No	-	1.1
Mn	Sibelco (calcined)	Fresh-calcined	SCFC	No	-	1.7
		After-used	SCAU	No	-	2.1
	Elwaleed B	Fresh-calcined	EBFC	No	-	4.2
		After-used	EBAU	No	-	4.3

The results show that iron-based oxygen carriers defluidized under a highly reducing environment, while the manganese-based materials did not. LD slag was an exception; still, one should consider that this material has a rather low iron content compared to the other iron-based oxygen carriers, see Table 3.1. Furthermore, all the oxygen carriers that defluidized did so during the oxidation period after being heavily reduced.

The crystalline phases of the defluidized oxygen carriers are provided in Table 4.2 and an example of the XRD diffractograms is provided in Figure 4.3; the rest can be seen in Paper I. All the non-fresh materials were at reduced conditions when they were analyzed with XRD.

Table 4.2 The main phases in the defluidized oxygen carriers at various mass conversion degrees confirmed by XRD.

Sample	Degree of reduction (%)	Fe ₂ O ₃ ^A (hematite)	Fe ₂ TiO ₅ ^B (pseudo-brookite)	Fe ₃ O ₄ ^C (magnetite)	FeTiO ₃ ^D (pure ilmenite)	FeO ^E (wüstite)	Fe ^F (elemental iron)
ILFC	Calcined	✓	✓	-	-	-	-
	1.1	-	✓	-	-	-	-
	2.2	✓	-	✓	-	-	-
	3.2 (defluidized)	-	-	✓	✓	✓	✓
ILAU	After-used	✓	-	✓	-	-	-
	1.4	-	✓	✓	-	-	-
	2.5	-	✓	✓	-	✓	-
	3.7 (defluidized)	-	-	-	-	✓	✓
TOFC	Calcined	✓	-	-	-	-	-
	1.0	✓	-	✓	-	-	-
	2.9	-	-	✓	-	✓	-
	4.0 (defluidized)	-	-	✓	-	✓	✓

✓: the phase was identified, -: the phase was not identified

occur and cause the bed defluidization. The bed sintering can even take place in a much lower temperature, known as the Tamman temperature [70]. Table 4.3 below provides the melting temperature of relevant iron-based phases.

Table 4.3 The melting points of several iron-based phases

Phases	Melting point, T_m (°C)
Fe_2O_3	1565
Fe_3O_4	1597
$FeTiO_3$	1470
FeO	1377
Fe	1538

The sintering point of a pure metal solid solution was found to be between $0.67 - 0.75 T_m$, but that of a mixed metal powder could be even lower [71]. Given that the oxygen carriers used in this study are not pure, it could be understood that sintering might have taken place between the oxygen carrier particles. This can contribute to the bed defluidization that was observed during the investigation.

Furthermore, the structure of oxygen carrier may change during the reduction, especially concerning the distribution of iron. The analysis was carried out by comparing what the elemental distribution within an oxygen carrier particle looked like before and after defluidization. Figure 4.4 below illustrates the change in the elemental distribution detected under SEM/EDX.

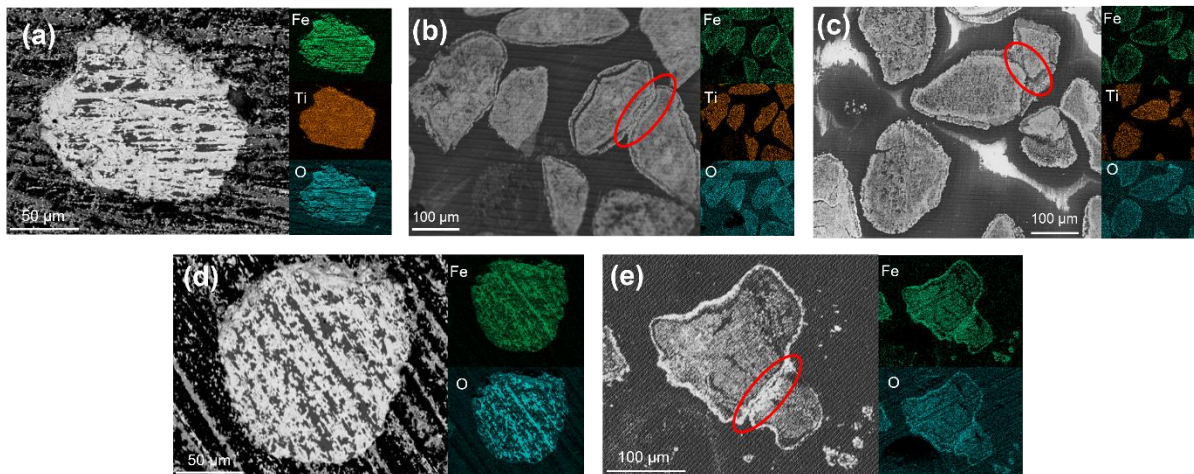


Figure 4.4 The elemental distribution of iron, titanium, and oxygen within (a) fresh ILFC, (b) defluidized ILFC, (c) defluidized ILAU, (d) fresh TOFC, and (e) defluidized TOFC. The red circles indicate interparticle joints.

In both ilmenite and Tiera ore, iron clearly migrated toward the outer surface of the oxygen carrier particles when defluidization occurred. This demonstrated the structural changes taking place under a highly reducing environment. The layers are likely iron that melted, as explained above, and formed interparticle joints, which then caused agglomeration and eventually defluidization. On the other hand, oxygen also showed some denser clusters on the surface, which might indicate that the layers still probably comprise some iron oxides. A previous study found the same pattern of iron migration under highly reducing conditions [24], [72].

A very high reduction degree may not be relevant in normal chemical-looping combustion, yet such a situation may occur, at least locally, in a system where the partial oxidation of fuel is required, e.g., in CLG, or in certain local zones of a reactor. Therefore, this knowledge will be useful in such a situation.

4.4 The reactivity of solid fuel toward oxygen carriers

The reactivity of pine forest residue char during a steam char conversion in the fluidized bed batch reactor was investigated using two iron-based oxygen carriers: ilmenite (Paper III) and iron sand (Paper II). Ilmenite can be considered as the benchmark chemical-looping oxygen carrier and many extensive studies have been performed on this material to investigate its performance and suitability as an oxygen carrier; the material has also been used as an oxygen carrier in large scale OCAC units [73]. Iron sand, on the other hand, is a new oxygen carrier candidate that is less explored and that has just recently been studied in a fluidized bed system in Paper II. Comparing the reactivity of a biomass-based char toward both materials in this thesis is thus highly interesting, especially at higher reduction degrees. In CLG, for instance, one can expect that the oxygen carrier will only be partially oxidized in the air reactor. This is done to maintain the partial oxidation of fuel during the gasification in the fuel reactor. Figure 4.5 compares both the hydrogen partial pressure and char conversion rate toward ilmenite and iron sand in the fluidized bed batch reactor, as well as the validation of three Langmuir – Hinshelwood mechanism models, at various mass conversion degrees.

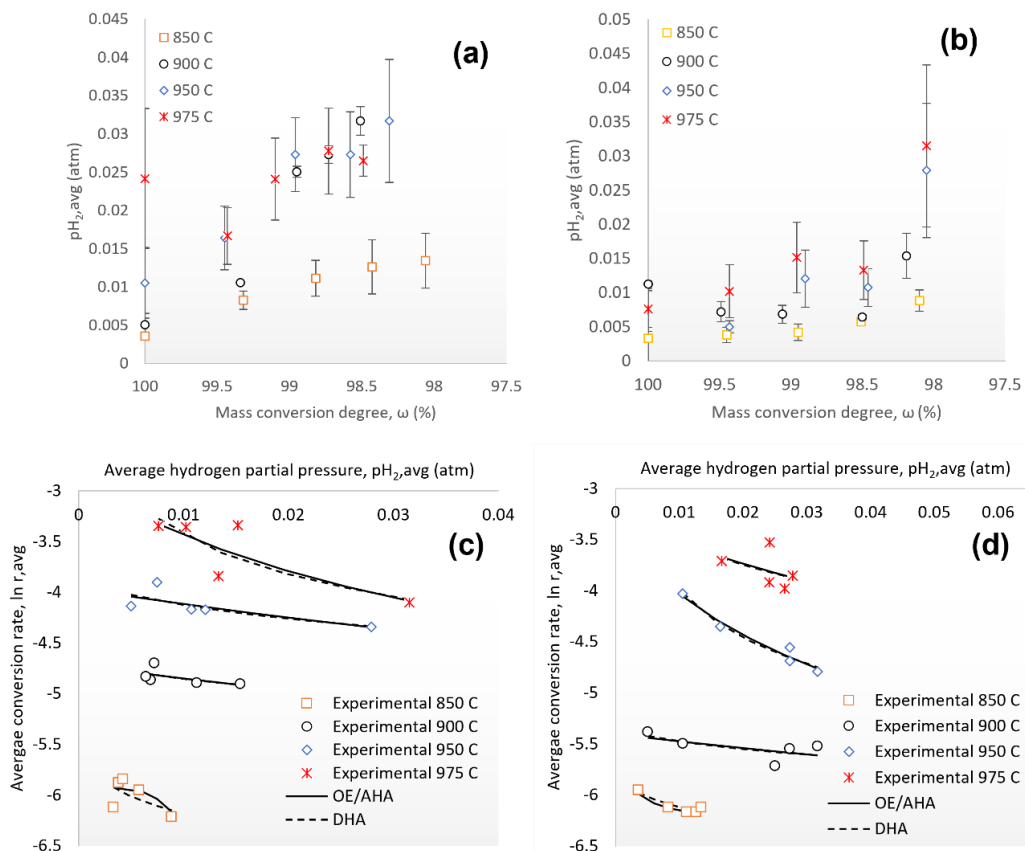


Figure 4.5 The hydrogen partial pressure during pine forest residue char conversion as a function of mass conversion degree, which was set by diluted CO injection, using (a) ilmenite and (b) iron sand as oxygen carriers. The conversion rate of the char using (c) ilmenite and (d) iron sand is plotted as a function of the hydrogen partial pressure to validate the Langmuir – Hinshelwood mechanism models.

In general, hydrogen partial pressure increases as oxygen carriers were pre-reduced further by diluted CO. The hydrogen generated from the char conversion using ilmenite does not differ significantly from that using iron sand. The hydrogen partial pressure caused by changes in the mass conversion degree alone was quite low; this could be due to the high dilution by steam and nitrogen. Still, the study was able to confirm that the mass conversion degree did affect the hydrogen partial pressure, especially at higher temperatures of 950 and 975 °C; the lower the mass conversion degree was, the higher hydrogen partial pressure became. This could be due to the equilibrium shift in the water-gas shift reaction [74] shown in Equation (1.4), which was caused by the exhausting available oxygen in the oxygen carrier.

Another possible explanation is that the reactivity of oxygen carriers has decreased at higher reduction degrees, as reflected by the declining char conversion rate. Thus, the char conversion rate did become lower at higher hydrogen partial pressures. This can be clearly seen on the conversion of pine forest char using ilmenite and iron sand at 975 °C and ≥ 950 °C, respectively. This indicates that a higher hydrogen partial pressure led to a slower char conversion rate, which is known as the hydrogen inhibition effect [66]. Since the hydrogen partial pressure was confirmed as a function of mass conversion degree, it means the mass conversion degree had an indirect effect on the char conversion rate; the lower the mass conversion degree was, the higher the hydrogen partial pressure and the lower the char conversion rate.

The mechanism of hydrogen inhibition can be predicted by validating three Langmuir – Hinshelwood mechanism models, see Table 3.9, against the experimental data. This can be seen in Figure 4.5c and 4.5d. The obtained model parameters are provided in Table 4.4 below; note that the oxygen exchange (OE) and associative hydrogen adsorption (AHA) share the same rate formula.

Table 4.4 The obtained Langmuir – Hinshelwood model parameters for ilmenite and iron sand

Model	Rate equation and units	Material	Parameters			
			850 °C	900 °C	950 °C	975 °C
OE/AHA	$r = \frac{1}{a + bpH_2}$ a in s, b in s.atm ⁻¹	Ilmenite	a = 313.6 b = 18,296	a = 111.4 b = 1,621	a = 52.6 b = 876	a = 17.8 b = 1,325
		Iron sand	a = 369 b = 8,215	a = 222 b = 1,630	a = 28 b = 2,813	a = 26 b = 794
DHA	$r = \frac{1}{a + b\sqrt{pH_2}}$ a in s, b in s.atm ^{-0.5}	Ilmenite	a = 224.5 b = 2,597	a = 95.2 b = 329.6	a = 41 b = 211	a = - 4.6 b = 356
		Iron sand	a = 304 b = 1,497	a = 195 b = 440	a = -25 b = 788	a = 10 b = 229

The validation shows that both OE/AHA and DHA models are close to each other, making it difficult to pinpoint which models are relevant. Based on the validation of the models in the conversion using ilmenite at 850 °C, it seems that OE/AHA fit the experimental data better than DHA; however, this cannot be used as a conclusion for all available data in both experiments using ilmenite and iron sand. One can only reflect from a previous study, where Lussier et al. [75] investigated an annealed char in a temperature programmed desorption (TPD). The study suggested that all adsorbable hydrogen had already been consumed at 727 °C, eliminating the possibility for AHA and DHA at higher temperatures. Despite the different char used in this thesis, the finding is considered relevant given the fact that all the temperatures

used in this study were higher than 727 °C. Therefore, the oxygen exchange mechanism was likely the relevant explanation of the hydrogen inhibition effect in this thesis for both materials.

Given the discussion, it seems that there is no significant difference between the reactivity of pine forest residue char toward ilmenite and that toward iron sand. The use of ilmenite in CLG has been recommended in Paper III based on the reactivity results and physical performance observation, e.g. no defluidization was observed during the experiments despite the high reduction degree. Hence, iron sand with similar reactivity and fluidization performance will likely show a good performance in CLG, and thus it can also be endorsed based on this finding.

5. Conclusions

This thesis explores how high reduction degrees of oxygen carrier may affect the performance and behavior of the material in multiple aspects. Several conclusions can be made:

- i) The syngas conversion of all oxygen carriers was high at high oxidation degrees and decreased at higher reduction degrees; an exceptionally quick reactivity decline was observed with the low-iron-containing by-product materials (iron sand and LD slag).
- ii) The reactivity of oxygen carriers toward methane decreased as the materials were priorly reduced further by syngas. Iron sand and LD slag, the by-product-based oxygen carriers, showed an exceptionally rapid decrease in CO₂ gas yield from methane. LD slag, however, released more CO than iron sand and even ilmenite at high oxidation degrees ($\omega > 99\%$).
- iii) A highly reducing environment may cause a defluidization of an oxygen carrier particle bed when iron ores were used. This is due to the formation of wüstite and/or elemental iron on the particles' surface, which may trigger bed agglomeration.
- iv) Manganese ores seem to be less prone to defluidization compared to the iron ores under a highly reducing environment.
- v) The conversion rate of pine forest residue char declined as the oxygen carriers, namely ilmenite and iron sand, were reduced to a higher extent. This is due to the increase in the hydrogen partial pressure, which caused a hydrogen inhibition effect.
- vi) There were no significant differences between ilmenite and iron sand with respect to the reactivity of pine forest residue char or defluidization tendency. The use of ilmenite and iron sand in CLG can therefore be recommended based on this finding.

Abbreviations and Nomenclatures

AR	Air reactor
AHA	Associative hydrogen adsorption
CLC	Chemical-looping combustion
CLG	Chemical-looping gasification
CLOU	Chemical-looping oxygen uncoupling
DHA	Dissociative hydrogen adsorption
EBAU	Elwaleed B manganese ore, in after – used form
EBFC	Elwaleed B manganese ore, in fresh – calcined form
FR	Fuel reactor
ILAU	Ilmenite, in after – used form
ILFC	Ilmenite, in fresh – calcined form
LDAU	LD slag, in after – used form
LDFC	LD slag, in fresh – calcined form
M_i	molecular weight of element i (gram/mole)
m_{ox}	mass of a fully oxidized sample (gram)
\dot{n}	gas molar flow (mol/second)
OC	Oxygen carrier
OE	Oxygen exchange
p_{H_2}	Hydrogen partial pressure (atm)
r	gasification rate
SCAU	Sibelco manganese ore (calcined), in after – used form
SCFC	Sibelco manganese ore (calcined), in fresh form
t	time (second)
TOFC	Tierga ore, in fresh – calcined form
T_m	melting point ($^{\circ}C$)
X_c	fraction of char conversion
x_i	molar fraction of species i
γ_i	gas yield of component i
ω	mass conversion degree

References

- [1] R. Cassia, M. Nocioni, N. Correa-Aragunde, and L. Lamattina, "Climate change and the impact of greenhouse gasses: CO₂ and NO, friends and foes of plant oxidative stress," *Front. Plant Sci.*, vol. 9, no. March, pp. 1–11, 2018.
- [2] United Nations, "Summary of the Paris Agreement," *United Nations Framew. Conv. Clim. Chang.*, pp. 27–52, 2015.
- [3] G. Gowrisankaran *et al.*, "Intermittency and the Value of Renewable Energy," *Natl. Bur. Econ. Res. Work. Pap.*, vol. 17086, 2011.
- [4] M. Rosso Grossman, "Climate Change and the Individual," *Am. J. Comp. Law*, vol. 66, no. 2017, pp. 345–378, 2018.
- [5] P. Zakkour, J. Kemper, and T. Dixon, "Incentivising and accounting for negative emission technologies," *Energy Procedia*, vol. 63, pp. 6824–6833, 2014.
- [6] K. Chen, R. C. Winter, and M. K. Bergman, "Carbon dioxide from fossil fuels: Adapting to uncertainty," *Energy Policy*, vol. 8, no. 4, pp. 318–330, 1980.
- [7] J. A. Mathews, "Carbon-negative biofuels," *Energy Policy*, vol. 36, no. 3, pp. 940–945, 2008.
- [8] A. I. Osman, M. Hefny, M. I. A. Abdel Maksoud, A. M. Elgarahy, and D. W. Rooney, "Recent advances in carbon capture storage and utilisation technologies: a review," *Environ. Chem. Lett.*, vol. 19, no. 2, pp. 797–849, 2021.
- [9] H. A. Alalwan and A. H. Alminshid, "CO₂ capturing methods: Chemical looping combustion (CLC) as a promising technique," *Sci. Total Environ.*, vol. 788, p. 147850, 2021.
- [10] P. Breeze, "Carbon Capture and Storage," in *Coal-Fire Generation*, Oxford: Elsevier Ltd., 2015, pp. 73–86.
- [11] S. Mukherjee, P. Kumar, A. Yang, and P. Fennell, "Energy and exergy analysis of chemical looping combustion technology and comparison with pre-combustion and oxy-fuel combustion technologies for CO₂ capture," *J. Environ. Chem. Eng.*, vol. 3, no. 3, pp. 2104–2114, 2015.
- [12] I. Staničić, T. Mattisson, R. Backman, Y. Cao, and M. Rydén, "Oxygen carrier aided combustion (OCAC) of two waste fuels - Experimental and theoretical study of the interaction between ilmenite and zinc, copper and lead," *Biomass and Bioenergy*, vol. 148, no. January, 2021.
- [13] P. Wang, H. Leion, and H. Yang, "Oxygen-Carrier-Aided Combustion in a Bench-Scale Fluidized Bed," *Energy and Fuels*, vol. 31, no. 6, pp. 6463–6471, 2017.
- [14] A. Abad, "Chemical looping for hydrogen production," in *Calcium and Chemical Looping Technology for Power Generation and Carbon Dioxide (CO₂) Capture*, Elsevier, 2015, pp. 327–374.
- [15] Z. Huang *et al.*, "Biomass char direct chemical looping gasification using NiO-modified iron ore as an oxygen carrier," *Energy and Fuels*, vol. 28, no. 1, pp. 183–191, 2014.
- [16] F. Hildor, H. Leion, C. J. Linderholm, and T. Mattisson, "Steel converter slag as an oxygen carrier for chemical-looping gasification," *Fuel Process. Technol.*, vol. 210, no. June, p. 106576, 2020.
- [17] Z. Yu *et al.*, "Iron-based oxygen carriers in chemical looping conversions: A review," *Carbon Resour. Convers.*, vol. 2, no. 1, pp. 23–34, 2019.
- [18] F. Störner, F. Lind, and M. Rydén, "Oxygen carrier aided combustion in fluidized bed boilers in Sweden—review and future outlook with respect to affordable bed materials," *Appl. Sci.*, vol. 11, no. 17, 2021.
- [19] T. Mattisson, "Materials for Chemical-Looping with Oxygen Uncoupling," *ISRN Chem. Eng.*, vol. 2013, no. 1, pp. 1–19, 2013.

- [20] Q. Imtiaz, D. Hosseini, and C. R. Müller, “Review of Oxygen Carriers for Chemical Looping with Oxygen Uncoupling (CLOU): Thermodynamics, Material Development, and Synthesis,” *Energy Technol.*, vol. 1, no. 11, pp. 633–647, 2013.
- [21] V. Purnomo, D. Yilmaz, H. Leion, and T. Mattisson, “Study of defluidization of iron- and manganese-based oxygen carriers under highly reducing conditions in a lab-scale fluidized-bed batch reactor,” *Fuel Process. Technol.*, vol. 219, no. December 2020, p. 106874, 2021.
- [22] S. Sundqvist, N. Khalilian, H. Leion, T. Mattisson, and A. Lyngfelt, “Manganese ores as oxygen carriers for chemical-looping combustion (CLC) and chemical-looping with oxygen uncoupling (CLOU),” *J. Environ. Chem. Eng.*, vol. 5, no. 3, pp. 2552–2563, 2017.
- [23] M. Arjmand, H. Leion, T. Mattisson, and A. Lyngfelt, “Investigation of different manganese ores as oxygen carriers in chemical-looping combustion (CLC) for solid fuels,” *Appl. Energy*, vol. 113, pp. 1883–1894, 2014.
- [24] J. Adánez, O. Condori, L. F. de Diego, F. Garcia-Labiano, M. T. Izquierdo, and A. Abad, “Syngas production in a 1.5 kWth biomass chemical looping gasification unit using Fe and Mn ores as the oxygen carrier,” *Energy and Fuels*, vol. 35, no. 21, pp. 17182–17196, 2021.
- [25] J. A. Medrano, H. P. Hamers, G. Williams, M. van Sint Annaland, and F. Gallucci, “NiO/CaAl₂O₄ as active oxygen carrier for low temperature chemical looping applications,” *Appl. Energy*, vol. 158, pp. 86–96, 2015.
- [26] M. A. Pans, P. Gayán, A. Abad, F. García-Labiano, L. F. De Diego, and J. Adánez, “Use of chemically and physically mixed iron and nickel oxides as oxygen carriers for gas combustion in a CLC process,” *Fuel Process. Technol.*, vol. 115, pp. 152–163, 2013.
- [27] F. Donat, W. Hu, S. A. Scott, and J. S. Dennis, “Characteristics of Copper-based Oxygen Carriers Supported on Calcium Aluminates for Chemical-Looping Combustion with Oxygen Uncoupling (CLOU),” *Ind. Eng. Chem. Res.*, vol. 54, no. 26, pp. 6713–6723, 2015.
- [28] M. Johansson, T. Mattisson, and A. Lyngfelt, “Comparison of oxygen carriers for chemical-looping combustion,” *Therm. Sci.*, vol. 10, no. 3, pp. 93–107, 2006.
- [29] C. Kuang, S. Wang, S. Lv, J. Cai, M. Luo, and J. Zhao, “Comparison of metallic oxide, natural ore and synthetic oxygen carrier in chemical looping combustion process,” *Int. J. Hydrogen Energy*, vol. 46, no. 34, pp. 18032–18041, 2021.
- [30] H. Tian, R. Siriwardane, T. Simonyi, and J. Poston, “Natural Ores as Oxygen Carriers in Chemical Looping Combustion,” 2013.
- [31] E. Ksepko, J. Klimontko, and A. Kwiecinska, “Industrial wastewater treatment wastes used as oxygen carriers in energy generation processes A green chemistry approach,” *J. Therm. Anal. Calorim.*, vol. 138, no. 6, pp. 4247–4260, 2019.
- [32] T. Mendiara, L. F. De Diego, P. Gayán, A. Abad, and J. Adánez, “Behaviour of a bauxite waste material as oxygen carrier in a 500 W th CLC unit with coal,” *Int. J. Greenh. Gas Control*, vol. 17, pp. 170–182, 2013.
- [33] V. Stenberg, M. Rydén, T. Mattisson, and A. Lyngfelt, “Experimental Investigation of Oxygen Carrier Aided Combustion (OCAC) with Methane and PSA Off-Gas,” *Appl. Sci.*, vol. 11, no. 210, 2021.
- [34] A. R. Bidwe, F. Mayer, C. Hawthorne, A. Charitos, A. Schuster, and G. Scheffknecht, “Use of ilmenite as an oxygen carrier in Chemical Looping Combustion-Batch and continuous dual fluidized bed investigation,” *Energy Procedia*, vol. 4, pp. 433–440, 2011.
- [35] H. Leion, A. Lyngfelt, M. Johansson, E. Jerndal, and T. Mattisson, “The use of ilmenite as an oxygen carrier in chemical-looping combustion,” *Chem. Eng. Res. Des.*, vol. 86,

- no. 9, pp. 1017–1026, 2008.
- [36] A. Cuadrat, A. Abad, J. Adánez, L. F. De Diego, and P. Gayán, “Behavior of ilmenite as oxygen carrier in chemical-looping combustion,” *Fuel Process. Technol.*, vol. 94, no. 1, pp. 101–112, 2012.
- [37] M. Vigoureux, T. Leffler, P. Knutsson, and F. Lind, “Sulfur capture and release by ilmenite used as oxygen carrier in biomass combustor,” *Fuel*, vol. 309, no. May 2021, p. 121978, 2022.
- [38] N. Berguerand, A. Lyngfelt, T. Mattisson, and P. Markström, “Chemical Looping Combustion of Solid Fuels in a 10 kW th Unit,” vol. 66, no. 2, pp. 181–191, 2011.
- [39] M. Keller, H. Oka, and J. Otomo, “Reactivity improvement of ilmenite by calcium nitrate melt infiltration for Chemical Looping Combustion of biomass,” *Carbon Resour. Convers.*, vol. 2, no. 1, pp. 51–58, 2020.
- [40] A. Lyngfelt and C. Linderholm, “Chemical-Looping Combustion of Solid Fuels – status and recent progress,” *Energy Procedia*, vol. 114, no. November 2016, pp. 371–386, 2017.
- [41] Y. Feng, Q. Yang, Z. Zuo, S. Luo, D. Ren, and H. Lin, “Study on Preparation of Oxygen Carrier Using Copper Slag as Precursor,” *Front. Energy Res.*, vol. 9, no. November, pp. 1–7, 2021.
- [42] Z. Huang *et al.*, “Emissions of nitrogenous pollutants in chemical looping gasification of high nitrogen wood waste using a K-modified copper slag oxygen carrier,” *J. Therm. Anal. Calorim.*, 2022.
- [43] N. Dong *et al.*, “Chemical looping gasification of sewage sludge using copper slag modified by NiO as an oxygen carrier,” *Chinese J. Chem. Eng.*, vol. 29, pp. 335–343, 2021.
- [44] F. Hildor, H. Leion, C. J. Linderholm, and T. Mattisson, “Steel converter slag as an oxygen carrier for chemical-looping gasification,” *Fuel Process. Technol.*, vol. 210, 2020.
- [45] F. Hildor, T. Mattisson, H. Leion, C. Linderholm, and M. Rydén, “Steel converter slag as an oxygen carrier in a 12 MWth CFB boiler – Ash interaction and material evolution,” *Int. J. Greenh. Gas Control*, vol. 88, no. July, pp. 321–331, 2019.
- [46] M. Rydén, M. Hanning, and F. Lind, “Oxygen Carrier Aided Combustion (OCAC) of wood chips in a 12 MWth circulating fluidized bed boiler using steel converter slag as bed material,” *Appl. Sci.*, vol. 8, no. 12, 2018.
- [47] G. L. Schwebel, H. Leion, and W. Krumm, “Comparison of natural ilmenites as oxygen carriers in chemical-looping combustion and influence of water gas shift reaction on gas composition,” *Chem. Eng. Res. Des.*, vol. 90, no. 9, pp. 1351–1360, 2012.
- [48] F. Guo *et al.*, “Catalytic reforming of biomass pyrolysis tar using the low-cost steel slag as catalyst,” *Energy*, vol. 189, p. 116161, 2019.
- [49] T. Mendiara, A. Abad, L. F. de Diego, F. García-Labiano, P. Gayán, and J. Adánez, “Reduction and oxidation kinetics of Tierga iron ore for Chemical Looping Combustion with diverse fuels,” *Chem. Eng. J.*, vol. 359, no. November 2018, pp. 37–46, 2019.
- [50] T. Mendiara, L. F. De Diego, F. García-Labiano, P. Gayán, A. Abad, and J. Adánez, “On the use of a highly reactive iron ore in Chemical Looping Combustion of different coals,” *Fuel*, vol. 126, pp. 239–249, 2014.
- [51] T. Mendiara, F. García-Labiano, A. Abad, D. Knittler, J. Y. Kim, and N. Ellis, “Air jet attrition measurements at hot conditions of oxygen carriers for chemical looping combustion,” *Powder Technol.*, vol. 392, pp. 661–671, 2021.
- [52] A. Hedayati, A. H. Soleimanisalim, C. J. Linderholm, T. Mattisson, and A. Lyngfelt, “Experimental evaluation of manganese ores for chemical looping conversion of synthetic biomass volatiles in a 300 W reactor system,” *J. Environ. Chem. Eng.*, vol. 9,

- no. 2, 2021.
- [53] D. Mei, C. Linderholm, and A. Lyngfelt, "Performance of an oxy-polishing step in the 100 kWth chemical looping combustion prototype," *Chem. Eng. J.*, vol. 409, no. December 2020, p. 128202, 2021.
- [54] M. Schmitz and C. Linderholm, "Chemical looping combustion of biomass in 10- and 100-kW pilots - Analysis of conversion and lifetime using a sintered manganese ore," *Fuel*, vol. 231, no. May, pp. 73–84, 2018.
- [55] D. Mei, A. H. Soleimanisalim, C. Linderholm, A. Lyngfelt, and T. Mattisson, "Reactivity and lifetime assessment of an oxygen releasable manganese ore with biomass fuels in a 10 kWth pilot rig for chemical looping combustion," *Fuel Process. Technol.*, vol. 215, no. February, p. 106743, 2021.
- [56] H. Leion, T. Mattisson, and A. Lyngfelt, "Use of ores and industrial products as oxygen carriers in chemical-looping combustion," *Energy and Fuels*, vol. 23, no. 4, pp. 2307–2315, 2009.
- [57] M. Rydén, H. Leion, T. Mattisson, and A. Lyngfelt, "Combined oxides as oxygen-carrier material for chemical-looping with oxygen uncoupling," *Appl. Energy*, vol. 113, pp. 1924–1932, 2014.
- [58] P. Hallberg *et al.*, "Experimental investigation of CaMnO_{3-δ} based oxygen carriers used in continuous chemical-looping combustion," *Int. J. Chem. Eng.*, vol. 2014, no. 1, 2014.
- [59] M. Q. ul I. Zafar, "Oxygen Carriers Materials for Chemical-Looping Technologies - Reactivity and Kinetics," 2007.
- [60] A. Di Giuliano, S. Lucantonio, and K. Gallucci, "Devolatilization of residual biomasses for chemical looping Gasification in Fluidized Beds Made up of Oxygen-Carriers," *Energies*, vol. 14, no. 2, 2021.
- [61] K. S. Pragadeesh and D. R. Sudhakar, "Color Indistinction Method for the Determination of Devolatilization Time of Large Fuel Particles in Chemical Looping Combustion," *Energy and Fuels*, vol. 33, no. 5, pp. 4542–4551, 2019.
- [62] G. Azimi, M. Keller, A. Mehdipoor, and H. Leion, "Experimental evaluation and modeling of steam gasification and hydrogen inhibition in Chemical-Looping Combustion with solid fuel," *Int. J. Greenh. Gas Control*, vol. 11, pp. 1–10, 2012.
- [63] R. Zhang, Q. H. Wang, Z. Y. Luo, M. X. Fang, and K. F. Cen, "Competition and Inhibition Effects during Coal Char Gasification in the Mixture of H₂O and CO₂," *Energy & Fuels*, vol. 27, no. 9, pp. 5107–5115, 2013.
- [64] K. J. Hüttinger, "Mechanism of water vapor gasification at high hydrogen levels," *Carbon N. Y.*, vol. 26, no. 1, pp. 79–87, 1988.
- [65] R. Zhang, Q. H. Wang, Z. Y. Luo, M. X. Fang, and K. F. Cen, "Competition and Inhibition Effects during Coal Char Gasification in the Mixture of H₂O and CO₂," *Energy & Fuels*, vol. 27, no. 9, pp. 5107–5115, 2013.
- [66] K. J. Hüttinger and W. F. Merdes, "The carbon-steam reaction at elevated pressure: Formations of product gases and hydrogen inhibitions," *Carbon N. Y.*, vol. 30, no. 6, pp. 883–894, 1992.
- [67] A. Akhtar, V. Krepl, and T. Ivanova, "A Combined Overview of Combustion, Pyrolysis, and Gasification of Biomass," *Energy and Fuels*, vol. 32, no. 7, pp. 7294–7318, 2018.
- [68] N. Z. Muradov, "How to produce hydrogen from fossil fuels without CO₂ emission," *Int. J. Hydrogen Energy*, vol. 18, no. 3, pp. 211–215, 1993.
- [69] D. R. Gaskell and D. E. Laughlin, *Introduction to the Thermodynamics of Materials*, 6th ed. Boca Raton: CRC Press, Taylor & Francis, 2018.
- [70] Q. Imtiaz, A. Armutlulu, F. Donat, M. A. Naeem, and C. R. Müller, "Preventing Agglomeration of CuO-Based Oxygen Carriers for Chemical Looping Applications," *ACS Sustain. Chem. Eng.*, vol. 9, no. 17, pp. 5972–5980, 2021.

- [71] P. S. Liu and G. F. Chen, "Making Porous Metals," in *Porous Materials*, 1st ed., Waltham: Elsevier Inc., 2014, pp. 21–112.
- [72] O. Condori, F. García-Labiano, L. F. de Diego, M. T. Izquierdo, A. Abad, and J. Adánez, "Biomass chemical looping gasification for syngas production using ilmenite as oxygen carrier in a 1.5 kWth unit," *Chem. Eng. J.*, vol. 405, no. July 2020, p. 126679, 2021.
- [73] H. Thunman, F. Lind, C. Breitholtz, N. Berguerand, and M. Seemann, "Using an oxygen-carrier as bed material for combustion of biomass in a 12-MWth circulating fluidized-bed boiler," *Fuel*, vol. 113, no. x, pp. 300–309, 2013.
- [74] N. Stolte, J. Yu, Z. Chen, D. A. Sverjensky, and D. Pan, "Water-gas shift reaction produces formate at extreme pressures and temperatures in deep earth fluids," *J. Phys. Chem. Lett.*, vol. 12, no. 17, pp. 4292–4298, 2021.
- [75] M. G. Lussier, Z. Zhang, and D. J. Miller, "Characterizing rate inhibition in steam/hydrogen gasification via analysis of adsorbed hydrogen," *Carbon N. Y.*, vol. 36, no. 9, pp. 1361–1369, 1998.